THE ASTROPHYSICAL JOURNAL, 486:132–146, 1997 September 1

OPTICAL AND FAR-INFRARED EMISSION OF *IRAS* SEYFERT GALAXIES[1]

CHARLES J. BONATTO AND MIRIANI G. PASTORIZA
Departamento de Astronomia, Instituto de Física, Universidade Federal do Rio Grande do Sul, C.P. 15051, CEP 91501-970, Porto Alegre, Rio Grande do Sul, Brazil

Received 1997 January 8; accepted 1997 April 3

ABSTRACT

This paper presents an analysis of moderately large samples of type 1 and 2 Seyfert galaxies through optical observations and far-infrared *IRAS* data, also taking into account theoretical color indices derived from dust emission models. The galaxies in the samples cover a rather large interval in far-infrared luminosity, i.e., $7.6 \leq \log (L_{IR}/L_{\odot}) \leq 12.6$. We show that both types of Seyferts have approximately the same distribution of number of objects with a given L_{IR}. Galaxies with similar far-infrared color indices $\alpha(100, 60)$ are grouped together, and the corresponding average color indices are interpreted in terms of a simple model in which the observed colors result from the combination of dust directly heated by the active galactic nucleus with a component from the host galaxy represented by the emission of cool dust. On the basis of the average *IRAS* colors of the derived groups, we show that type 1 and 2 Seyfert galaxies are undistinguishable from each other. From the luminosity ratios $L_{IR}/L_{H\alpha}$ and $L_{IR}/L_{[O\ III]}$, we show that basically the same model can be applied to both types of Seyfert, only allowing for the variation of model conditions: type 2 Seyferts would be like type 1 Seyferts but with the Seyfert nucleus and broad line region more effectively "hidden" by dust.

Subject headings: dust, extinction — galaxies: photometry — galaxies: Seyfert — infrared: galaxies

1. INTRODUCTION

The continuum energy distribution emitted by the central sources in active galactic nuclei (AGNs) joins to the radio region through the infrared. In recent years, with the use of better detectors, it has been observed that AGNs are, in general, very luminous in the infrared. Although the continuum spectrum of AGNs has been under intense study in the past two decades, the origins of the often complex features observed in the optical and infrared regions are not yet fully understood.

Since the discovery of the strong infrared excess in NGC 1068 (Pacholczyck & Wisniewski 1967), there have been debates on whether Seyfert galaxies emit in the infrared predominantly by thermal reradiation from dust grains or what is measured is directly the extension into the infrared of the UV/optical continuum emitted by the central ionizing source (CIS) lying at the cores of these objects. The observation of emission and absorption features similar to those in Galactic thermal sources (at 3.3, 7.7, 8.6, and 11.3 μm, and the silicates feature at 10 μm) in a reasonably large number of luminous Seyfert galaxies (Roche et al. 1984; Jones et al. 1984) has led to the conclusion that at least some fraction of the infrared flux comes from thermal reradiation.

Observational evidence for the presence of dust in nuclear regions of AGNs is substantial, and several examples can be found in the following references: Rudy (1984), MacAlpine (1985), and Ward et al. (1987). High Balmer decrements measured in some Seyferts, which cannot be interpreted only in terms of recombination processes and interstellar reddening, are consistent with the presence of small solid particles that redden the nuclear continuum and emission lines. Intensity ratios of [S II] blends at λ4072 and λ10320 (Wampler 1968, 1971) also show the presence of dust along the line of sight. Even in low- and intermediate-luminosity quasars, dust is detectable (Rudy 1984).

Neugebauer et al. (1976) and Rieke (1978) point out a tendency of the infrared spectra of Seyfert 2 galaxies to fall very rapidly toward higher frequencies and be very steep near 3 μm, whereas the nonstellar spectra of Seyfert 1 galaxies are relatively intense in the region 1–3 μm and can be fitted by a power law of moderate slope through the interval 1–20 μm. They conclude that the Seyfert 2 continuum strongly suggests that the infrared excess is due to reradiation by dust, whereas in the Seyfert 1 a nonthermal source should be dominant.

With the introduction of more accurate analytical models consisting of dust grains being heated directly by the UV/optical continuum from the CIS, first proposed by Rees et al. (1969), the continuum spectrum of some radio-quiet quasars could be reasonably well fitted with a combination of this thermal source (plus a flat power-law optical continuum) with a "cool" component coming from the host galaxy (Barvainis 1990).

In the present work we study a moderately large sample of type 1 and 2 Seyferts with far-infrared data taken from the *IRAS* Point Source Catalogue (Joint *IRAS* Science Working Group 1985). Part of this sample has been observed in the optical region. Global properties of these galaxies are interpreted with theoretical color indices taken from a dust emission model that also includes the effects of a "cold" component from the host galaxy.

This paper is structured as follows: § 2 presents the galaxy samples, § 3 discusses the far-infrared properties of our galaxies, § 4 presents the dust emission model and discusses the optical and far-infrared luminosities, and § 5 summarizes our conclusions.

2. GALAXY SAMPLES

One of the goals of this work is to compare type 1 and 2 Seyferts in the optical and far-infrared spectral ranges. In order to perform statistically significant analyses, we have

[1] Based partly on observations made at Cerro Tololo Inter-American Observatory and Complejo Astronomico El Leoncito.

searched the literature for the largest possible number of galaxies with *IRAS* observations and reliable optical line luminosities, with no other specific selection criterion.

Galaxies from two samples are used in the analysis: the optical spectra of 38 *IRAS* galaxies selected from the catalog of AGN candidates of de Grijp, Miley, & Lub (1987; sample A) and a compilation of *IRAS* flux densities and optical luminosities for 336 type 1 and 2 Seyferts selected from the literature (sample B). Since $\approx 90\%$ of the galaxies in samples A and B have been classified as warm *IRAS* sources by de Grijp et al. (1987, 1992), our combined sample can be considered to be essentially flux limited at both 25 and 60 μm, and a small bias may be present in the sense that it favors warmer *IRAS* Seyferts. For the sake of increasing the number of objects, we included a few cases ($\approx 4\%$ of the combined sample) with only the *IRAS* fluxes available, with detection in at least two bands. Finally, since many of the warm *IRAS* sources listed by de Grijp et al. (1987) as potential Seyferts still do not have optical spectra available (especially the weaker ones), our sample cannot be considered complete in any way.

Optical spectra ($\approx \lambda\lambda 3700$–$7000$) for galaxies in sample A were obtained with the Z-MACHINE (Tonry & Davis 1979) at the Cassegrain focus of the 2.15 m telescope of Complejo Astronomico El Leoncito (CASLEO, Argentina), in the period 1989 May–November by S. Lipari, and with the 2D-FRUTTI attached to the Cassegrain focus of the 1.0 m telescope of Cerro Tololo Inter-American Observatory (CTIO, Chile). in two runs in 1990 May and September by C. Bonatto and Th. Storchi-Bergmann. Resolutions typically of the order of FWHM ≈ 4.5 Å were obtained in the final spectra.

Table 1 gathers relevant information on the galaxies of sample A: the columns give the identification of each galaxy, coordinates (relative to 1950), the redshift z (measured from the position of narrow forbidden lines observed in our spectra), and flux densities (in janskys) at the *IRAS* bands, where an "L" indicates upper limit detec-

TABLE 1

DATA FOR SAMPLE A GALAXIES

				S_ν (Jy)				log $(L/L_\odot)$			
GALAXY	α(1950)	δ(1950)	z	12 μm	25 μm	60 μm	100 μm	[O III]	Hα	L_{IR}^W	L_{IR}^C
Seyfert 1 Galaxies											
ESO 543−G11	01 37 51.0	−22 30 16	0.0866	0.13	0.29	0.51	0.53L	8.80	11.60	11.60	11.35
ESO 362−G18	05 17 44.0	−32 42 30	0.0122	0.22	0.57	1.40	1.99	7.66	7.83	10.20	10.07
NGC 6860.....	20 04 29.0	−61 14 42	0.0148	0.24	0.33	0.95	2.47	7.92	8.75	10.16	10.19
UGC 12138	22 37 46.5	07 47 34	0.0248	0.20	0.34	0.83	2.48L	8.47	8.78	10.60	10.61
Seyfert 2 Galaxies											
NGC 34	00 08 33.4	−12 23 08	0.0184	0.36	2.38	16.08	16.97	7.47	7.98	11.45	11.45
IRAS 0019−7926.....	00 19 55.6	−79 26 52	0.0729	0.28	1.15	3.10	2.87	8.60	8.42	12.12	11.96
IC 1657	01 11 46.6	−32 54 55	0.0124	0.20L	0.27	2.77	7.48	6.55	6.77	10.30	10.50
ESO 353−G9.....	01 29 33.4	−33 22 36	0.0158	0.18	0.30	2.16	5.76	7.40	7.58	10.44	10.61
IRAS 0135−1307.....	01 35 37.9	−13 07 25	0.0405	0.12	0.50	0.93	1.18	8.40	8.25	11.15	10.94
ESO 153−G20	02 04 20.0	−55 25 52	0.0200	0.10	0.19	0.89	3.02L	7.00	6.95	10.32	10.48
ESO 545−G13	02 22 20.2	−19 21 59	0.0331	0.17	0.35	1.45	3.64	8.49	8.29	11.00	11.08
IC 1816	02 29 47.8	−36 53 29	0.0170	0.16	0.39	1.39	2.33	8.25	8.17	10.41	10.39
UGC 2024.....	02 30 27.2	00 12 05	0.0218	0.25	0.84	2.49	2.54	8.14	8.03	10.92	10.79
ESO 199−IG23	03 10 59.6	−51 31 58	0.0782	0.09L	0.18	0.51	0.92	8.74	8.35	11.40	11.34
ESO 200−IG9.....	03 20 12.0	−51 50 15	0.0577	0.18	0.40	0.51	0.56	8.37	8.07	11.31	10.98
ESO 116−G18	03 23 52.6	−60 54 50	0.0181	0.18	0.64	1.46	1.98	7.35	7.63	10.58	10.43
NGC 1365.....	03 31 41.0	−36 18 24	0.0059	4.42	13.07	84.20	142.5	6.84	7.74	11.18	11.24
IRAS 0336−1641.....	03 36 15.7	−16 42 01	0.0373	0.21	0.50	1.06	2.01L	7.75	7.58	11.10	10.99
ESO 420−G13	04 11 53.3	−32 07 58	0.0114	0.52	2.13	14.17	21.61	7.32	7.70	10.98	11.03
ESO 033−G2.....	04 57 36.0	−75 37 00	0.0180	0.21	0.45	0.68	2.08L	7.45	7.45	10.34	10.25
ESO 362−G8.....	05 09 20.0	−34 27 12	0.0158	0.07	0.18	0.64	1.50L	7.50	7.61	10.01	10.05
NGC 4748.....	12 49 35.2	−13 08 36	0.0142	0.17	0.37	1.16	2.22	7.81	8.04	10.20	10.17
NGC 4903.....	12 58 39.0	−30 59 54	0.0163	0.11L	0.29	0.77	2.40	...	7.16	10.17	10.22
IRAS 1548−0344.....	15 48 04.0	−03 44 18	0.0309	0.18	0.73	1.07	4.05L	8.30	7.89	11.03	10.98
Frl 49	18 32 32.5	−59 26 40	0.0196	0.62	1.38	3.23	3.90	8.80	9.02	10.99	10.83
IC 4729	18 34 45.0	−67 28 18	0.0145	0.12	0.16	1.43	4.48	...	6.83	10.16	10.39
ESO 338−IG4.....	19 24 29.0	−41 40 36	0.0094	0.07L	0.42	1.69	1.01	7.84	7.50	9.96	9.82
IRAS 1958−1818.....	19 58 02.8	−18 18 47	0.0373	0.32	0.59	0.85	1.12	7.70	7.80	11.10	10.84
IC 4995	20 16 13.0	−52 46 48	0.0162	0.08	0.33	0.83	1.25	8.17	7.60	10.21	10.10
ESO 462−G9.....	20 18 44.0	−31 26 54	0.0192	0.13L	0.21L	0.75	1.30	7.51	8.01	10.25	10.23
IRAS 2020−5635.....	20 20 58.4	−56 35 09	0.0601	0.11L	0.28L	0.64	1.44L	8.73	8.41	11.30	11.24
II Zw 83	20 24 20.1	−02 26 35	0.0290	0.39	0.91	1.16	1.53	8.49	8.40	11.04	10.75
ESO 235−IG26	20 55 38.2	−52 12 02	0.0507	0.10L	0.30	1.30	1.33	8.75	8.28	11.33	11.26
ESO 599−G6.....	21 16 43.6	−20 38 56	0.0392	0.14L	0.31	1.79	2.28	7.12	8.08	11.19	11.20
IRAS 2136−2700.....	21 36 20.3	−27 00 08	0.0308	0.16L	0.28	1.17	1.39	7.89	8.12	10.84	10.79
MCG +03-58-07	22 46 55.9	−19 32 17	0.0316	0.28	0.79	2.42	3.36	8.71	8.45	11.23	11.15
UGC 12348	23 02 45.6	−00 04 45	0.0256	0.11	0.42L	0.96	1.56	7.96	7.84	10.70	10.58
NGC 7582.....	23 15 38.0	−42 38 36	0.0050	1.62	6.44	49.10	72.92	6.53	6.95	10.78	10.84

NOTE.—Units of right ascension are hours, minutes, and seconds, and units of declination are degrees, arcminutes, and arcseconds. Luminosities are calculated for $H_0 = 50$ km s^{-1} Mpc^{-1}; "L" stands for upper limit detection.

TABLE 2

DATA FOR THE SEYFERT 1 GALAXIES IN SAMPLE B

GALAXY	α (1950)	δ (1950)	z	S_ν (Jy)				log ($L/L_\odot$)			
				12 μm	25 μm	60 μm	100 μm	[O III]	Hα	L_{IR}^{W}	L_{IR}^{C}
Mrk 334	00 00 35.5	21 40 53	0.0220	0.25L	1.06L	4.19	4.33	7.43	7.94	11.10	11.02
Mrk 335	00 03 36.3	19 55 29	0.0250	0.34	0.48	0.45	0.85L	7.11	9.29	10.59	10.26
ESO 012−G21	00 39 16.0	−79 30 54	0.0310	0.25L	0.36	1.45	2.81	8.06	9.09	10.94	10.97
UGC 0524	00 48 53.1	29 07 46	0.0360	0.25	0.63	0.94	1.82:	...	...	11.10	10.91
I Zw 1	00 50 57.8	12 25 20	0.0609	0.51	1.21	2.24	2.63	9.06	9.97	11.90	11.69
Mrk 975	01 11 12.7	13 00 27	0.0500	0.37L	0.41L	0.78	1.42L	8.68	9.24	11.26	11.12
II Zw1	01 19 26.5	−01 18 05	0.0540	0.25L	0.45L	1.44	2.02	9.20	9.51	11.48	11.41
Mrk 357	01 19 57.0	22 54 35	0.0479	0.48	0.26	0.96	0.85	8.75	8.88	11.17	11.06
Mrk 358	01 23 45.0	31 21 25	0.0460	0.09	0.14L	0.32	1.26L	7.79	8.46	10.75	10.82
Mrk 359	01 24 50.1	18 55 07	0.0170	0.25L	0.55:	1.24	1.76	7.55	7.77	10.45	10.31
UGC 1395	01 52 44.6	06 22 06	0.0177	0.25	0.99	0.54	1.38	7.30	8.11	10.55	10.09
Mrk 1014	01 57 15.8	00 09 10	0.0162	0.25L	0.63	2.30	2.20	7.29	7.90	10.58	10.48
Mrk 590	02 12 00.4	−00 59 58	0.0270	0.30L	0.38L	0.53	1.41	7.63	8.08	10.61	10.47
Mrk 1040	02 25 14.5	31 05 23	0.0160	0.66	1.32	2.73	4.73	7.69	8.41	10.76	10.63
Mrk 1048	02 32 10.5	−09 00 21	0.0433	0.27L	0.58	1.43	1.91	7.55	9.34	11.33	11.20
ESO 416−G5	02 36 36.3	−31 01 14	0.0620	0.15	0.26	0.72	1.32	7.70	9.07	11.34	11.28
2S4U0241+61	02 41 01.3	62 15 27	0.0436	0.59	0.89:	0.79L	31.51L	9.89	11.09	11.35	11.98
Mrk 372	02 46 31.4	19 05 49	0.0310	0.13L	0.17	0.30	0.19L	8.96	...	10.43	10.13
IRAS 0255−167	02 55 21.6	−16 42 42	0.0680	0.11	0.29	0.92	0.91	...	...	11.50	11.38
UGC 2514	03 01 16.5	−01 17 53	0.0132	0.31	0.54	0.78	1.00L	6.45	6.28	10.14	9.87
1E 0412.5−0803	04 12 27.0	−08 03 08	0.0386	0.25L	0.54	0.66	1.00	9.03	9.18	11.07	10.78
NGC 1566	04 18 53.3	−55 03 23	0.0040	0.56	0.94	12.50	41.27	6.74	7.22	9.95	10.21
3C 120	04 30 31.6	05 15 00	0.0330	0.38	0.71	1.30	2.56	8.57	9.40	11.11	10.98
Mrk 618	04 33 59.9	−10 28 36	0.0356	0.34	0.79	2.71	4.24	8.37	9.15	11.37	11.32
IRAS 0444−052	04 44 52.2	−05 13 33	0.0442	0.39L	0.29	0.84	1.30L	7.70	8.58	11.08	11.01
IRAS 0449−646	04 49 21.3	−64 41 15	0.0600	0.20	0.28	0.36	0.57	8.13	8.48	11.19	10.92
UGC 3223	04 56 30.0	04 54 29	0.0180	0.25	0.31	1.67	3.10	7.12	8.00	10.48	10.54
Mrk 1095	05 13 37.9	−00 12 15	0.0330	0.40	0.48	0.65	1.31	7.78	9.33	10.89	10.68
IRAS 0520−122	05 20 20.7	−12 13 34	0.0490	0.11L	0.12	0.53	2.65L	8.70	9.29	10.90	11.17
IRAS 0521−122	05 21 48.6	−12 12 42	0.0490	0.10	0.28	0.43	1.02	8.71	9.35	11.03	10.89
MCG +8-11-11	05 51 09.7	46 25 51	0.0766	0.63	1.99	2.76	4.32	9.67	9.92	11.28	12.03
H0557−385	05 56 21.0	−38 20 15	0.0399	0.53	0.70	0.42L	1.00	8.09	9.33	11.13	10.69
UGC 3478	06 28 00.3	63 42 38	0.0123	0.25L	0.35	1.46	3.21	7.00	7.82	10.12	10.17
Mrk 6	06 45 43.9	74 29 10	0.0190	0.31L	0.68	1.11	0.94	8.49	9.01	10.58	10.29
Mrk 373	06 50 30.8	50 25 05	0.0200	0.14	0.25	1.77	2.66	...	...	10.56	10.62
Mrk 374	06 55 34.5	54 15 57	0.0440	0.11	0.19	0.27	0.68L	8.38	9.10	10.76	10.60
Frl 265	06 56 18.3	−65 29 28	0.0295	0.25L	0.19	0.78	1.13	7.43	8.34	10.63	10.60
Mrk 376	07 10 36.2	45 47 07	0.0560	0.35L	0.58	0.86	1.27L	7.98	9.51	11.47	11.23
Mrk 9	07 32 42.2	58 52 56	0.0390	0.30	0.53	0.87	1.47	7.17	9.27	11.12	10.93
Mrk 79	07 38 47.3	49 55 41	0.0220	0.31	0.78	1.49	2.09	8.48	8.62	10.80	10.62
Mrk 10	07 43 07.4	61 03 25	0.0300	0.25	0.30	0.84	2.13	7.06	8.97	10.74	10.75
Mrk 382	07 52 03.5	39 19 07	0.0340	0.15L	0.24L	0.21	0.74	7.55	8.03	10.56	10.34
1E 0754+39	07 54 38.3	39 28 36	0.0958	0.14L	0.28	0.17	0.72L	9.65	10.37	11.54	11.25
UGC 4155	07 57 17.7	26 45 07	0.0255	0.25L	0.44	0.99	1.51L	8.14	7.91	10.72	10.58
VII Zw 244	08 38 32.0	77 03 59	0.1323	0.09L	0.09	0.17	0.59L	8.65	...	11.51	11.50
NGC 2639	08 40 00.0	50 23 29	0.0110	0.35L	0.40L	1.99	6.79	6.29	7.35	10.13	10.31
NGC 2691	08 51 32.3	39 43 40	0.0130	0.37L	0.28L	1.28	3.43	...	6.74	10.10	10.21
Mrk 704	09 15 39.4	16 30 59	0.0290	0.44:	0.60	0.47L	1.00L	8.09	9.33	10.80	10.43
NGC 2841	09 18 35.9	51 11 24	0.0021*	0.90	0.83	4.41	24.21	...	5.14	9.13	9.45
Mrk 705	09 23 20.0	12 57 03	0.0280	0.25L	0.30L	0.67	1.56L	7.88	8.34	10.63	10.58
Mrk 124	09 45 24.3	50 43 29	0.0560	0.25L	0.29	0.67	1.00L	8.61	9.43	11.25	11.12
Mrk 1239	09 49 46.3	−01 23 35	0.0190	0.71	1.21	1.39	1.14	6.87	8.96	10.78	10.39
NGC 3031	09 51 30.0	69 18 18	0.0004*	0.25	0.25L	2.35	25.25	5.53	5.36	7.58	8.18
Mrk 141	10 15 39.3	64 13 06	0.0360	0.25L	0.25L	0.75	1.73	7.75	8.71	10.84	10.85
NGC 3227	10 20 46.8	20 07 06	0.0030*	0.67	1.75	7.84	16.93	7.00	7.27	9.79	9.85
Ton 524A	10 28 46.4	29 02 27	0.0600	0.25L	0.86	2.18	3.26	...	...	11.80	11.70
UGC 6100	10 58 42.0	45 55 29	0.0290	0.25L	0.26L	0.61	1.60	...	...	10.61	10.59
NGC 3516	11 03 22.8	72 50 20	0.0090	0.46	0.93	1.73	2.08	7.05	8.20	10.08	9.87
ESO 438−G9	11 08 22.0	−28 13 42	0.0243	0.37L	0.57	3.24	4.06	7.72	8.62	11.03	11.03
Mrk 734	11 19 10.9	12 00 47	0.0490	0.30L	0.48L	0.51	1.08L	8.38	...	11.21	10.94
Mrk 423	11 24 07.6	35 31 17	0.0320	0.28L	0.25L	1.36	2.20	7.68	7.52	10.90	10.93
NGC 3718	11 29 50.0	53 20 42	0.0030*	0.36L	0.62L	0.81L	2.81	5.74	5.12	8.89	8.79
NGC 3783	11 36 33.0	−37 27 41	0.0090	0.80	2.45	3.33	4.93	7.84	8.45	10.45	10.19
Mrk 42	11 51 05.7	46 29 24	0.0240	0.10L	0.14L	0.32	0.91	6.99	7.96	10.17	10.16
I Sz 96	11 58 06.0	−20 34 00	0.0619	0.25L	0.39L	1.67	2.38	...	...	11.62	11.60
NGC 4051	12 00 36.4	44 48 35	0.0020*	0.79	1.42	8.16	20.35	6.43	6.75	9.24	9.36
NGC 4235	12 14 36.7	07 28 09	0.0080	0.13L	0.16L	0.32	0.65	6.24	...	9.23	9.12
NGC 4253	12 15 55.6	30 05 26	0.0126	0.41	1.38	4.01	4.07	7.91	8.38	10.65	10.51
Mrk 205	12 19 31.8	75 35 10	0.0700	0.25L	0.66L	0.40L	1.31	8.81	9.74	11.62	11.26
NGC 4579	12 35 12.0	12 05 36	0.0060	0.38L	0.33L	4.46	17.38	5.64	6.21	9.85	10.16
NGC 4593	12 37 05.0	−05 04 12	0.0090	0.37	0.93	2.75	5.79	7.20	8.43	10.18	10.17

TABLE 2—*Continued*

Galaxy	α (1950)	δ (1950)	z	S_ν (Jy)				log ($L/L_\odot$)			
				12 μm	25 μm	60 μm	100 μm	[O III]	Hα	L_{IR}^{W}	L_{IR}^{C}
NGC 4594	12 37 23.0	−11 21 00	0.0020*	0.57L	0.43:	3.12	11.72	5.76	6.08	8.79	9.04
Mrk 231	12 54 05.0	57 08 38	0.0409	1.82	8.56	33.26	30.05	7.61	8.51	12.56	12.46
Mrk 236	12 58 18.1	61 55 26	0.0520	0.06L	0.09L	0.17	0.64L	7.92	8.68	10.63	10.65
NGC 5033	13 11 08.0	36 51 50	0.0030	0.78	1.06	13.08	43.55	6.18	6.16	9.72	9.99
Mrk 1347	13 20 25.0	08 25 20	0.0500	0.32L	0.50L	0.90	1.69:	7.72	8.83	11.33	11.18
IC 4271	13 27 06.9	37 40 19	0.0077	0.06L	0.12L	0.23	1.47L	6.93	7.71	9.06	9.23
IRAS 1332−340	13 32 59.0	−34 02 11	0.0075	0.40	0.81	1.12	1.00L	6.68	7.69	9.81	9.49
IC 4329A	13 46 27.9	−30 03 41	0.0140	1.06	2.27	2.01	1.55	7.87	9.22	10.75	10.27
PG 1351+640	13 51 46.2	64 00 28	0.0882	0.14	0.53	0.73	1.10	8.76	9.24	11.84	11.58
Mrk 279	13 51 52.5	69 33 16	0.0310	0.25L	0.31	1.08	2.49	8.24	9.29	10.84	10.87
IRAS 1404+286W	14 04 44.1	28 41 38	0.0769	0.40L	0.38	0.74	1.00L	8.10	9.20	11.62	11.44
I Zw 81	14 06 20.4	49 05 56	0.0520	0.28L	0.25L	0.49	1.08	7.52	7.76	11.08	10.99
NGC 5548	14 15 43.7	25 21 59	0.0170	0.38:	0.77	1.04	1.66	8.27	9.08	10.51	10.25
Mrk 471	14 20 46.9	33 04 37	0.0340	0.25L	0.33L	0.64	1.99	7.41	7.23	10.82	10.79
Mrk 1383	14 26 33.8	01 30.27	0.0865	0.13	0.21	0.24	0.38L	10.07	11.02	11.39	11.09
NGC 5683	14 33 06.1	48 52 47	0.0409	0.25L	0.25L	0.52	1.28	7.95	…	10.88	10.82
Mrk 817	14 34 57.8	59 00 39	0.0314	0.34	1.17	2.12	2.27	8.15	9.20	11.28	11.05
Mrk 478	14 40 04.8	35 38 56	0.0783	0.25L	0.25L	0.59	1.02	8.90	10.02	11.50	11.40
Mrk 668	14 40 45.6	28 41 29	0.0769	0.18L	0.40	0.73	0.94	8.66	9.66	11.63	11.43
Mrk 1388	14 48 23.0	22 56 23	0.0213	0.15L	0.23	0.17	0.57	8.12	7.80	10.10	9.82
ESO 448−G10	14 55 44.7	−28 30 19	0.0481	0.31	0.38	0.67	0.78	8.22	8.14	11.17	10.94
Mrk 841	15 01 36.3	10 37 56	0.0363	0.39L	0.45	0.51	1.00	8.69	9.54	10.92	10.66
Mrk 845	15 06 12.5	51 38 41	0.0420	0.25L	0.25L	0.40L	1.09	7.74	8.03	10.85	10.75
IRAS 1509−211	15 09 06.8	−21 07 46	0.0446	0.23	0.50	1.52	1.55	8.59	9.25	11.34	11.21
IRAS 1519+393	15 19 39.6	39 22 45	0.0292	0.10	0.15	0.46	0.78	7.70	7.93	10.44	10.39
NGC 5940	15 28 51.3	07 37 38	0.0330	0.25L	0.25L	0.78	1.71:	7.63	8.62	10.78	10.78
Mrk 290	15 34 44.8	58 04 00	0.0296	0.11L	0.14L	0.17	0.58	8.61	…	10.24	10.12
IRAS 1543+272	15 43 52.6	27 15 49	0.0310	0.05L	0.12	0.69	0.85	6.99	7.35	10.57	10.57
Mrk 291	15 52 54.0	19 20 16	0.0350	0.07L	0.09L	0.34	0.98L	7.71	8.25	10.43	10.53
Mrk 493	15 57 16.6	35 10 13	0.0310	0.25L	0.29	0.64	1.29	7.33	8.29	10.71	10.62
Mrk 867	16 00 03.3	26 28 06	0.0724	0.20	0.18	0.56	1.40	7.98	8.84	11.35	11.37
Mrk 871	16 06 15.6	12 27 41	0.0340	0.25L	0.41	0.81	1.04:	7.90	8.74	10.92	10.73
Mrk 876	16 13 36.3	65 50 38	0.0127	0.25L	0.25	0.63	1.06:	9.31	10.18	9.88	9.79
NGC 6104	16 14 40.1	35 49 50	0.0280	0.25L	0.25L	0.54	1.69	…	…	10.55	10.55
Mrk 699	16 22 05.3	41 11 48	0.0342	0.14L	0.08L	0.24	0.63L	8.15	8.62	10.30	10.33
Mrk 1498	16 24 48.5	51 53 05	0.0563	0.25L	0.30	0.41:	1.00L	9.06	…	11.17	11.00
IRAS 1626+518	16 26 47.9	51 53 04	0.0547	0.13	0.29	0.38	0.32	8.59	8.70	11.12	10.78
VII Zw 653	16 36 00.0	85 36 00	0.0627	0.27L	0.32:	0.46	1.00L	7.92	9.05	11.31	11.13
Mrk 700	17 01 21.1	31 31 26	0.0340	0.25L	0.33	2.19	2.56	7.23	8.00	11.14	11.15
UGC 10683B	17 02 24.7	−01 28 23	0.0310	0.25L	0.30L	0.56	1.56	7.38	8.35	10.69	10.63
IRAS 1721+365SW	17 21 39.3	36 33 03	0.0400	0.14	0.14	0.34	0.81	8.22	8.67	10.64	10.61
CSV 163	17 47 18.0	68 36 58	0.0626	1.15L	0.25L	0.44	2.61L	8.34	9.02	11.23	11.36
IRAS 1829+412N	18 29 57.9	41 13 53	0.0922	0.06	0.19	0.39	0.68	8.87	9.34	11.50	11.37
ESO 103−G35	18 33 22.0	−65 28 18	0.0133	0.58	2.38	2.25	1.46	7.39	7.58	10.73	10.26
Frl 51	18 40 15.0	−62 24 54	0.0142	0.47L	1.03	1.84	2.75	7.80	8.46	10.52	10.33
3C 390.3	18 45 37.6	79 43 06	0.0570	0.25L	0.29	0.40L	1.00L	8.84	9.63	11.17	11.01
ESO 141−G55	19 16 57.0	−58 45 54	0.0360	0.24	0.35	0.57	1.48L	8.44	9.62	10.86	10.75
NGC 6814	19 39 55.8	−10 26 33	0.0052	0.49L	0.60	5.52	18.88	6.61	6.38	9.85	10.10
Mrk 509	20 41 26.2	−10 54 17	0.0353	0.35	0.75	1.40	1.37	8.88	9.87	11.20	10.96
Mrk 896	20 43 44.5	−02 59 47	0.0270	0.25	0.25	0.63	1.53	7.45	8.49	10.55	10.52
IRAS 2121−179	21 21 54.0	−17 57 43	0.1123	0.29L	0.41	1.14	1.26	8.40	9.53	12.09	11.96
II Zw 136	21 30 01.2	09 55 01	0.0617	0.29	0.45	0.52	1.00L	9.07	9.93	11.41	11.14
Mrk 516	21 53 52.8	07 07 43	0.0280	0.39L	0.31L	1.35	2.18	6.58	7.32	10.81	10.81
NGC 7213	22 06 08.5	−47 24 45	0.0050	0.63	0.74	2.56	8.63	6.57	7.63	9.61	9.73
NGC 7214	22 06 30.0	−28 05 10	0.0227	0.25L	0.50:	2.10	5.03	7.56	8.48	10.82	10.89
IRAS 2211−393	22 11 45.0	−39 03 13	0.0394	0.40L	0.45	0.77	1.04L	7.55	8.83	11.06	10.85
3C 445	22 21 14.7	−02 21 25	0.0562	0.21	0.26	0.31	1.03L	8.99	9.37	11.09	10.95
Mrk 915	22 34 07.3	−12 48 17	0.0241	0.17L	0.35	0.46	1.01	8.47	8.53	10.47	10.27
Ark 564	22 40 18.3	29 27 47	0.0250	0.25L	0.57	1.00	1.11	8.05	8.76	10.76	10.52
IRAS 2241−608	22 41 57.0	−60 49 48	0.1130	0.14	0.32	0.45	0.52	9.14	…	11.85	11.56
NGC 7469	23 00 44.5	08 36 18	0.0170	1.30	5.50	26.67	34.40	8.62	9.28	11.65	11.63
Mrk 315	23 01 35.8	22 21 13	0.0400	0.39L	0.41	1.49	2.73L	7.82	8.56	11.20	11.20
NGC 7603	23 16 22.7	−00 01 48	0.0290	0.36	0.48L	0.82	2.03	7.79	8.66	10.81	10.71
UM 163	23 27 58.0	−02 44 20	0.0320	0.25	0.31L	0.73	1.27	7.05	…	10.78	10.68
Mrk 541	23 53 28.4	07 14 42	0.0410	0.14L	0.18L	0.35	1.19	7.60	8.48	10.72	10.72

Note.—Units of right ascension are hours, minutes, and seconds, and units of declination are degrees, arcminutes, and arcseconds. Luminosities are calculated for $H_0 = 50$ km s^{-1} Mpc^{-1}; "L" stands for upper limit detection, a colon (:) indicates uncertain value, and an asterisk (*) following the redshift value indicates the objects for which the distance has been calculated via the distance modulus (Sandage & Tammann 1981).

TABLE 3

DATA FOR THE SEYFERT 2 GALAXIES IN SAMPLE B

GALAXY	α (1950)	δ (1950)	z	S_ν (Jy)				log ($L/L_\odot$)			
				12 μm	25 μm	60 μm	100 μm	[O III]	Hα	L_{IR}^{W}	L_{IR}^{C}
IRAS 0016−073	00 16 03.6	−07 19 28	0.0178	0.22	0.61	1.68	1.36	6.15	6.96	10.58	10.41
IRAS 0032−003	00 32 10.6	−00 18 55	0.0420	0.09	0.31	0.89	1.02	7.30	7.01	11.07	10.94
IRAS 0033−819E	00 33 18.5	−81 56 32	0.1271	0.07	0.23	0.58	0.91	8.73	...	11.94	11.83
Mrk 955.....	00 35 08.1	00 00 21	0.0350	0.25L	0.41L	0.94	2.05:	7.67	8.04	10.97	10.91
Mrk 957.....	00 39 09.7	40 04 51	0.0370	0.25L	0.28	2.14	3.33	6.69	7.73	11.19	11.25
Mrk 348.....	00 46 04.9	31 41 04	0.0159	0.34	0.78	1.43	1.75	8.01	7.55	10.51	10.29
IRAS 0052−709	00 52 06.0	−70 54 21	0.0688	0.29	0.85	1.11	1.00L	8.61	8.49	11.80	11.46
ESO 541−IG12.....	00 59 50.0	−19 56 18	0.0560	0.25L	0.29	0.72	1.01	7.87	7.68	11.26	11.14
IRAS 0107−038	01 07 13.5	−03 48 25	0.0546	0.27L	0.66	1.05	1.00L	9.15	8.60	11.51	11.23
Tol 109−383	01 09 09.8	−38 20 56	0.0109	1.09	1.77	1.83	1.95	7.98	7.97	10.44	10.05
IRAS 0111+849	01 11 52.9	84 55 54	0.0564	0.25L	0.72	1.30	1.74	7.57	7.54	11.60	11.40
Mrk 1	01 13 19.6	32 49 33	0.0160	1.80	0.81	2.28:	2.73	7.99	7.51	10.62	10.50
ESO 195−G35.....	01 13 45.0	−50 27 00	0.0170	0.25	1.78	0.66	1.54	6.99	7.85	10.74	10.13
NGC 513	01 21 37.3	33 32 22	0.0160	0.25L	0.29L	1.83	4.08	7.63	8.24	10.39	10.51
NGC 526A	01 21 42.0	−35 20 00	0.0180	0.29	0.52	0.36L	0.85L	7.99	7.36	10.30	9.92
Mrk 993.....	01 22 42.7	31 52 35	0.0170	0.25L	0.73L	0.40L	1.23	6.99	6.96	10.38	9.97
Mrk 1157	01 30 38.9	35 24 45	0.0150	0.25L	0.46	1.97	3.19	7.76	7.54	10.42	10.42
MCG +02-05-022	01 34 37.5	−09 24 12	0.0698	0.17	0.28	0.82	1.16	7.84	7.92	11.49	11.40
V Zw 85.....	01 37 35.7	31 59 38	0.0650	0.27L	0.30L	0.75L	1.44	...	...	11.42	11.35
Mrk 573.....	01 41 22.9	02 05 56	0.0172	0.25L	0.93L	1.09	1.26	8.72	8.25	10.58	10.24
IRAS 0147−076	01 47 33.7	−07 40 36	0.0177	0.33	0.82	1.16	0.41	7.27	7.44	10.58	10.18
IRAS 0147+359	01 47 35.2	35 54 33	0.0808	0.25L	0.32	0.61	1.00L	8.25	8.24	11.59	11.43
Frl 377	02 09 01.0	−49 56 04	0.0475	0.25L	0.17	0.58	1.43	8.03	7.63	10.96	11.00
ESO 197−G27.....	02 09 02.0	−49 55 50	0.0460	0.25L	0.26	0.58	1.37	8.00	7.82	11.02	10.96
NGC 1068	02 40 07.1	−00 13 31	0.0030*	38.30	86.83	185.58	238.70	7.96	7.39	11.12	10.95
NGC 1097	02 44 12.0	−30 29 00	0.0040	1.85	5.83	45.49	82.53	5.44	6.51	10.55	10.65
Mrk 1058	02 46 47.0	34 46 54	0.0180	0.25L	0.26L	0.66	1.45	7.31	7.12	10.20	10.16
NGC 1144	02 52 38.0	−00 23 10	0.0290	0.33	0.71	5.23	11.21	6.59	6.43	11.36	11.48
IRAS 0253−166	02 53 42.7	−16 41 18	0.0315	0.25L	0.29	0.72	1.44	8.09	8.09	10.74	10.68
Mrk 1066	02 56 49.0	36 37 18	0.0120	0.50	2.32	10.28	12.71	7.59	7.88	10.94	10.90
MCG +02-08-039	02 58 04.0	−11 36 55	0.0296	0.29L	0.49	0.56	0.77	8.26	7.56	10.78	10.45
NGC 1229	03 05 59.0	−23 08 50	0.0350	0.28	0.81	1.54	1.86	8.52	10.03	11.23	11.02
IRAS 0310−029	03 10 36.5	−02 54 29	0.0272	0.41L	0.42	1.10	1.01L	7.29	7.13	10.79	10.62
Mrk 1073	03 11 42.9	41 51 03	0.0230	0.47	1.43	8.11	11.42	8.12	8.02	11.38	11.39
IRAS 0312+013	03 12 38.0	01 19 25	0.0233	0.25L	0.28	0.85	1.99	7.57	7.38	10.51	10.52
NGC 1320	03 22 17.8	−03 13 05	0.0091	0.33	1.06	2.15	2.75	7.12	6.80	10.17	9.98
Mrk 609.....	03 22 57.3	−06 19 09	0.0343	0.29L	0.48	2.55	4.76	7.97	8.67	11.24	11.29
IRAS 0323−580	03 23 01.2	−58 00 46	0.0437	0.12L	0.17	0.66	0.48	7.11	7.17	10.92	10.80
IRAS 0327−434W.....	03 27 49.8	−43 29 14	0.0584	0.25L	0.37	1.26	1.95	7.69	7.76	11.48	11.44
Mrk 612.....	03 28 09.9	−03 18 35	0.0199	0.25L	0.30L	1.13	1.77	7.91	7.73	10.45	10.43
NGC 1358	03 31 10.8	−05 15 24	0.0134	0.08L	0.12L	0.38	0.92	7.41	7.06	9.66	9.68
IRAS 0333−564S.....	03 33 34.6	−56 25 08	0.0785	0.27L	0.54	1.36	1.42	8.71	8.51	11.85	11.69
NGC 1386	03 34 51.0	−36 09 47	0.0020*	0.50	1.45	5.82	9.54	7.35	6.86	9.94	9.93
IRAS 0335+010S.....	03 35 35.0	01 04 29	0.0396	0.25L	0.46	0.67	1.00L	8.13	7.68	11.05	10.81
NGC 1409	03 38 38.0	−01 27 44	0.0247	0.25L	0.25L	0.86	2.00	7.37	8.50	10.54	10.57
IRAS 0357−615	03 57 30.7	−61 32 29	0.0474	0.25L	0.45	1.53	2.65	8.35	8.16	11.38	11.35
IRAS 0422−254	04 22 59.1	−25 28 09	0.0436	0.27L	0.32	1.11	1.32	7.82	7.77	11.16	11.08
IRAS 0438−084	04 38 30.5	−08 28 06	0.0150	0.42	1.62	2.77	2.53	6.29	6.52	10.76	10.49
ESO 118−IG33.....	04 39 12.9	−59 46 36	0.0577	0.27L	0.20	0.47	1.03L	7.73	7.73	11.12	11.06
NGC 1667	04 46 10.0	−06 24 20	0.0150	0.40	0.67	5.77	14.21	6.13	6.89	10.80	10.97
NGC 1685	04 50 02.8	−03 01 29	0.0140	0.38	0.39L	1.06	1.69	6.95	6.85	10.17	10.09
IRAS 0450−032	04 50 13.9	−03 17 56	0.0157	0.12	0.38	0.83	1.22	7.05	6.95	10.22	10.07
IRAS 0450+039	04 50 47.2	03 58 47	0.0297	0.27	0.58	0.66	1.00L	8.43	8.10	10.85	10.54
UGC 3255	05 07 10.0	07 25 29	0.0190	0.25	0.25	1.12	2.49	...	...	10.38	10.44
ESO 253−G03.....	05 23 53.1	−46 02 52	0.0439	0.24	1.01	2.80	2.97	8.33	8.36	11.61	11.47
NGC 2110	05 49 46.4	−07 28 02	0.0070	0.39	0.89	4.39	6.08	6.97	7.18	10.08	10.08
IRAS 0559−579	05 59 34.6	−57 56 19	0.0383	0.25L	0.23	0.77	1.01	8.02	7.78	10.89	10.82
Mrk 3	06 09 48.4	71 03 11	0.0140	0.70	2.86	3.88	3.35	8.37	7.97	10.91	10.57
IRAS 0611−326	06 11 30.3	−32 40 59	0.0500	0.25L	0.28	0.83	1.13	8.08	7.98	11.19	11.10
VII Zw 73	06 25 38.0	63 42 39	0.0402	0.25L	0.50	1.76	2.46	8.13	7.96	11.28	11.23
IRAS 0627+689E	06 27 23.0	68 58 11	0.0650	0.37L	0.29	0.85	1.15L	7.75	7.63	11.44	11.34
IRAS 0629−664	06 29 12.7	−66 27 59	0.0466	0.08L	0.18	0.71	1.06	8.37	7.83	11.00	10.98
ESO 287−G26.....	06 31 43.6	−64 03 45	0.0485	0.26L	0.25	0.57	0.99	8.04	7.75	11.05	10.94
NGC 2273	06 45 37.5	60 54 13	0.0060	0.46	1.37	6.24	9.91	6.75	6.59	10.11	10.12
Mrk 78	07 37 56.8	65 17 42	0.0380	0.25L	0.54	1.12	1.18	9.03	8.72	11.15	10.94
IRAS 0741+293	07 41 01.5	29 22 06	0.0160	0.28	0.34	0.63	1.95	...	...	10.15	10.12
Mrk 1210	08 01 27.0	05 15 22	0.0130	0.56	2.10	1.82	1.44	8.26	7.95	10.65	10.17
Mrk 622.....	08 04 21.0	39 08 59	0.0232	0.19L	0.40	1.28	1.43	7.38	7.52	10.67	10.57
MCG +10-12-090	08 07 48.8	58 06 06	0.0280	0.15	0.21	1.34	2.36	...	...	10.75	10.82
ESO 18−G09	08 25 33.5	−77 37 22	0.0175	0.28L	0.45	1.32	4.65	7.03	7.25	10.45	10.55
IRAS 0827−027	08 27 43.9	−02 42 47	0.0404	0.25L	0.42	1.52	1.82	8.35	8.04	11.22	11.15

TABLE 3—*Continued*

Galaxy	α (1950)	δ (1950)	z	S_ν (Jy)				log ($L/L_\odot$)			
				12 μm	25 μm	60 μm	100 μm	[O III]	Hα	L_{IR}^{W}	L_{IR}^{C}
MCG +01-24-012	09 18 17.8	−07 50 41	0.0198	0.14	0.48	0.74	1.06	7.59	7.34	10.46	10.22
IRAS 0930−841	09 30 31.9	−84 08 26	0.0628	0.25L	0.36	0.48	2.14	8.08	8.46	11.35	11.32
IRAS 0930+682	09 30 35.5	68 13 49	0.0703	0.10	0.26	0.45	1.15L	8.41	8.16	11.35	11.26
NGC 2992	09 43 17.4	−14 05 48	0.0070	0.60	1.38	6.76:	13.98	7.70	7.50	10.27	10.33
IRAS 0943−111	09 43 35.8	−13 07 10	0.1310	0.28L	0.42	0.52	1.00L	9.50	...	12.10	11.85
NGC 3079	09 58 35.0	55 55 15	0.0037*	2.62	3.58	50.17	10.34	...	6.22	10.57	10.52
NGC 3185	10 14 53.3	21 56 19	0.0041	0.15	0.14	0.43	3.67	5.77	...	8.68	9.05
IRAS 1021+675	10 21 34.6	67 32 58	0.0386	0.35L	0.43	0.77	1.43L	8.29	8.11	11.03	10.88
ESO 436−G09.....	10 28 05.0	−30 08 18	0.0136	0.15	0.19	1.38	3.32	6.62	...	10.11	10.26
NGC 3281	10 29 37.0	−34 35 48	0.0110	0.88	2.58	6.66	7.40	6.87	6.62	10.77	10.62
Mrk 34	10 30 51.4	60 17 22	0.0510	0.26	0.47	0.95	1.10	9.09	8.62	11.35	11.15
MCG +12-10-067	10 40 30.2	70 40 09	0.0328	0.25L	0.26	0.95	2.82	7.84	7.60	10.83	10.92
NGC 3393	10 46 00.0	−24 53 48	0.0120	0.25L	0.72	2.35	3.78	8.20	7.75	10.35	10.30
IRAS 1104−115	11 04 39.6	−11 22 55	0.0548	0.11L	0.19L	0.31	1.30L	8.91	8.67	10.98	10.99
IRAS 1105−115	11 05 48.4	−11 31 46	0.0548	0.25L	0.42	0.72	1.38L	8.82	8.54	11.33	11.17
NGC 3660	11 21 00.5	−08 23 16	0.0110	0.26L	0.25L	1.91	4.48	6.66	7.11	10.06	10.21
IRAS 1121−281	11 21 33.3	−28 06 38	0.0135	0.44L	0.31	0.59	1.00L	7.02	6.79	9.97	9.81
MCG +05-27-013	11 24 55.7	−28 59 02	0.0234	0.11	0.34	0.60	0.94	7.84	7.52	10.48	10.29
Mrk 176.....	11 29 54.3	53 13 30	0.0270	0.29L	0.28:	0.75	1.31L	8.16	7.84	10.61	10.54
MCG +10-17-021	11 33 01.9	57 13 49	0.0507	0.16	0.52	1.55	2.17	8.29	8.01	11.47	11.38
Mrk 1457	11 44 42.6	52 43 39	0.0490	0.25L	0.32L	0.89	1.12L	8.20	8.22	11.21	11.10
NGC 3982	11 53 52.1	55 24 10	0.0030*	0.49	0.84	6.83	15.45	6.44	...	9.72	9.87
Mrk 198.....	12 06 43.2	47 20 07	0.0240	0.25L	0.27L	0.63	2.20L	7.91	7.58	10.46	10.50
NGC 4388	12 23 14.0	12 56 20	0.0080	0.10	3.57	10.73	17.27	7.61	7.29	10.67	10.61
NGC 4438	12 25 13.6	13 17 07	0.0002*	0.17	0.16	4.28	12.05	...	8.47	9.32	9.59
NGC 4507	12 32 54.5	−39 38 02	0.0120	0.46	1.42	4.52	5.40	8.13	7.80	10.64	10.54
IC 3639	12 38 09.0	−36 29 20	0.0109	0.66	2.32	7.08	10.77	7.62	7.53	10.76	10.69
NGC 4704	12 46 25.0	42 11 37	0.0270	0.28L	0.48	1.70	2.32	7.88	7.11	10.91	10.85
IRAS 1246−111	12 46 51.6	−11 07 31	0.0477	0.19	0.74	1.50	2.27L	9.07	8.73	11.48	11.33
ESO 323−G32.....	12 50 30.2	−41 21 31	0.0162	0.25L	0.30	0.98	1.73	7.38	7.16	10.23	10.20
NGC 4826	12 54 16.9	21 57 18	0.0014	2.37	3.03	35.45	77.60	...	4.79	9.49	9.66
IRAS 1254−301	12 54 21.3	−30 06 22	0.0546	0.10	0.31	1.05	1.46	7.96	7.90	11.34	11.28
NGC 4922B	12 59 00.0	29 35 29	0.0240	0.32L	1.32	6.51	6.80	7.30	7.74	11.34	11.29
NGC 4941	13 01 37.0	−05 17 00	0.0030	0.25L	0.58L	1.31	3.95	6.35	5.94	8.96	8.96
NGC 4968	13 04 23.5	−23 24 31	0.0093	0.40	1.26	2.30	3.23	7.24	6.98	10.24	10.05
IRAS 1305−241	13 05 59.6	−24 07 00	0.0137	0.14L	0.67	1.44	1.49	6.14	6.28	10.34	10.14
NGC 5005	13 08 37.0	37 19 20	0.0033	0.66	1.09	18.47	58.25	4.96	5.61	9.93	10.20
IRAS 1314+451E	13 14 27.9	45 08 22	0.0905	0.25L	0.49	0.72	1.40L	8.87	8.71	11.84	11.64
IRAS 1319−164	13 19 42.3	−16 27 53	0.0167	0.86	2.81	5.61	5.61	8.67	8.22	11.12	10.90
NGC 5135	13 22 56.6	−29 34 24	0.0130	0.68	2.49	15.94	30.05	7.62	7.69	11.15	11.23
NGC 5194	13 27 46.0	47 27 20	0.0010*	1.37	2.40	31.68	121.42	5.37	5.13	9.65	9.96
IRAS 1329+022	13 29 19.1	02 16 30	0.0856	0.12	0.40	0.99	0.88	8.07	8.36	11.80	11.61
IRAS 1330−231	13 30 24.0	−23 17 16	0.0337	0.20L	0.23L	0.87	2.12	7.74	8.02	10.81	10.86
ESO 383−G18.....	13 30 34.7	−33 45 33	0.0128	0.25L	0.39	0.65	1.00L	7.44	7.26	10.00	9.79
IRAS 1331−234	13 31 51.2	−23 25 26	0.0087	0.25	0.37	0.91	1.72	6.46	6.66	9.71	9.64
IRAS 1331−231	13 31 56.4	−23 11 36	0.0446	0.98	0.63	0.89	1.60	8.26	7.98	11.29	11.07
UGC 8621	13 35 30.0	39 25 29	0.0200	0.25	0.28L	0.93	2.29	...	...	10.39	10.43
NGC 5256	13 36 14.6	48 31 53	0.0277	0.48L	1.03L	7.20	11.80	7.44	7.54	11.46	11.53
Mrk 268.....	13 38 54.0	30 37 49	0.0410	0.25L	0.28	1.42	1.71	8.11	7.60	11.15	11.13
Mrk 273.....	13 42 51.7	56 08 14	0.0378	0.23	2.30	22.10	22.44	8.58	8.65	12.20	12.23
IRAS 1345+125W.....	13 45 06.5	12 32 21	0.1202	0.25L	0.66	2.01	2.14	8.74	8.79	12.38	12.26
NGC 5347	13 51 04.0	33 44 15	0.0080	0.34	0.93	1.44	2.59	6.51	6.27	9.95	9.75
Tol 1351−375.....	13 51 18.0	−37 31 54	0.0520	0.11	0.32	0.45	1.25L	8.41	9.03	11.13	11.00
Mrk 463.....	13 53 39.9	18 36 57	0.0497	0.51	1.58	2.18	1.92	9.30	9.23	11.78	11.45
NGC 5427	14 00 49.0	−05 47 30	0.0087	0.34:	0.63:	4.77	15.96	7.16	6.49	10.25	10.48
IRAS 1408+137	14 08 16.6	13 47 33	0.0158	0.26L	1.04	3.64	2.85	6.89	7.20	10.77	10.64
NGC 5506	14 10 39.1	−02 58 26	0.0058	1.28	4.20	8.46	8.88	7.23	7.19	10.37	10.16
Mrk 673.....	14 15 06.1	27 05 15	0.0360	0.25	0.36	2.85	5.35	6.97	7.64	11.28	11.39
IRAS 1423−116	14 23 27.6	−11 40 37	0.0412	0.12L	0.30L	0.64	1.20	7.22	7.54	10.97	10.86
IRAS 1426+573	14 26 46.0	57 23 44	0.0428	0.11	0.19	0.51	0.95	8.06	7.71	10.85	10.79
NGC 5643	14 29 28.0	−43 57 15	0.0030	0.87	3.37	18.45	43.26	6.90	6.47	9.95	10.06
NGC 5674	14 31 22.5	05 40 38	0.0250	0.25L	0.36L	1.48	3.36	...	...	10.76	10.81
IRAS 1431−326	14 31 42.8	−32 37 19	0.0254	0.27L	0.32	0.94	1.00L	7.19	7.38	10.63	10.51
Mrk 477.....	14 39 02.5	53 43 04	0.0380	0.25L	0.54	1.35	1.77	9.40	9.01	11.18	11.05
NGC 5728	14 39 36.8	−17 02 22	0.0093	0.18	0.87	8.87	14.91	7.82	7.52	10.55	10.66
IRAS 1443+272	14 43 25.9	27 14 38	0.0294	0.25L	0.34	0.78	1.24	8.16	8.01	10.73	10.61
ESO 273−IG04.....	14 45 26.0	−43 43 25	0.0373	0.55	1.80	4.75	5.37	...	...	11.70	11.56
IRAS 1506+092	15 06 42.7	09 13 50	0.0450	0.25L	0.29	0.71	1.12	8.35	8.22	11.06	10.95
IRAS 1518+085	15 18 26.9	08 34 31	0.0306	0.18	0.25	0.82	1.55	7.86	8.01	10.72	10.70
MCG +11-19-006	15 18 44.7	65 45 59	0.0444	0.15	0.35	0.88	1.19	8.29	7.92	11.14	11.01
IRAS 1521+087	15 21 46.3	08 43 21	0.0364	0.25L	0.34	0.78	1.03L	7.29	7.57	10.93	10.78
IRAS 1524+117	15 24 04.5	00 46 04	0.0507	0.25	0.47	0.90	1.28:	8.02	7.77	11.33	11.15

TABLE 3—*Continued*

Galaxy	α (1950)	δ (1950)	z	S_ν (Jy)				log ($L/L_\odot$)			
				12 μm	25 μm	60 μm	100 μm	[O III]	Hα	L_{IR}^{W}	L_{IR}^{C}
NGC 5929	15 24 19.0	41 50 40	0.0080	0.40	1.63	9.30	13.26	6.83	6.96	10.50	10.52
IRAS 1529+242S	15 29 32.5	24 14 32	0.0961	0.10	0.34	1.07	1.06	8.85	8.50	11.89	11.77
IRAS 1530+302	15 30 26.2	30 17 55	0.0650	0.09	0.26	0.33	0.44	8.39	7.77	11.23	10.93
ESO 1530−085	15 30 37.0	−08 31 22	0.0230	0.25L	0.48:	1.94	3.48	8.28	8.47	10.80	10.81
NGC 5953	15 32 13.2	15 21 40	0.0073	0.57	1.08	10.24	19.71	6.93	7.16	10.41	10.54
IC 4553 (=Arp 220)	15 32 48.6	23 40 07	0.0180	0.48	8.15	103.68	116.25	6.19	6.71	12.19	12.25
UGC 9944	15 36 16.2	73 36 53	0.0248	0.29L	0.61	1.31	2.01	7.51	7.32	10.82	10.68
IRAS 1541+286	15 41 53.4	28 40 52	0.0320	0.25L	0.38	1.24	1.47	8.13	7.84	10.94	10.85
3C 327	15 59 54.1	02 06 30	0.1040	0.30L	0.38	0.60	1.00L	9.00	8.55	11.87	11.67
Mrk 883	16 27 47.1	24 33 06	0.0380	0.38L	0.31L	1.10	1.11	8.04	8.27	11.03	10.93
IRAS 1628+394S	16 28 50.8	39 29 25	0.0297	0.41L	0.18	0.69	1.00L	7.84	7.76	10.59	10.56
IRAS 1638−062W	16 38 12.1	−06 13 10	0.0279	0.20	0.27	0.88	0.73	7.39	7.74	10.67	10.53
NGC 6221	16 48 25.0	−59 08 00	0.0040	1.51	5.31	35.96	33.23	6.04	7.09	10.47	10.45
IRAS 1649+220N	16 49 13.0	22 00 27	0.0546	0.25L	0.45	0.99	0.94	7.88	8.07	11.41	11.20
IRAS 1702+457S	17 02 03.3	45 44 52	0.0604	0.25L	0.42	1.10	1.60	8.23	8.48	11.51	11.40
NGC 6300	17 12 18.0	−62 45 50	0.0030	0.75	2.17	13.80	39.35	6.32	5.77	9.81	9.97
IRAS 1712+395	17 12 29.1	39 33 17	0.0362	0.14	0.17	0.71	1.29	6.91	7.10	10.77	10.78
UGC 10889	17 29 41.7	59 40 33	0.0281	0.07	0.11	0.70	1.70	7.28	7.15	10.48	10.61
MCG +03-45-003	17 33 25.9	20 49 38	0.0240	0.25L	0.39	0.70	1.57	8.22	7.83	10.56	10.45
IRAS 1734+493W	17 34 53.6	49 20 17	0.0748	0.25L	0.30	0.79	1.06	8.23	8.13	11.56	11.44
IRAS 1737+562W	17 37 06.9	56 15 02	0.0646	0.25L	0.38	1.01	1.51	8.35	8.03	11.53	11.43
Mrk 507	17 48 55.4	68 42 50	0.0530	0.25L	0.25L	0.60	1.15	7.25	8.02	11.14	11.06
IRAS 1752+189	17 52 07.6	18 57 25	0.0395	0.09	0.18	0.69	1.06	6.72	7.43	10.85	10.82
IRAS 1759+423	17 59 36.5	42 21 37	0.0526	0.07L	0.15	0.63	0.69	8.47	8.08	11.05	10.99
IC 4769	18 43 00.5	−63 12 40	0.0151	0.23	0.76	4.38	8.15	7.52	...	10.73	10.80
IC 4777	18 44 11.0	−53 12 30	0.0187	0.27L	0.26L	0.71	1.44L	7.20	7.64	10.25	10.21
IRAS 1846+721	18 46 16.2	72 07 41	0.0461	0.25L	0.26	0.95	0.97	8.50	8.55	11.13	11.04
IRAS 1911−498	19 11 56.3	−49 52 59	0.0492	0.09L	0.31	0.89	0.89	6.96	7.37	11.21	11.07
Frl 513	19 18 25.0	−74 04 00	0.0700	0.25L	0.25L	1.74	1.96	...	...	11.69	11.70
NGC 6764	19 07 01.2	50 51 08	0.0081	0.36	1.29	6.33	11.56	6.32	7.31	10.37	10.41
IRAS 1918−578	19 18 37.4	−57 48 21	0.0587	0.06L	0.16	0.87	1.79	6.92	7.19	11.26	11.33
IRAS 1925−727	19 25 27.7	−72 45 39	0.0615	0.33	1.44	5.18	6.03	7.92	8.52	12.14	12.06
3C 405 (=Cyg A)	19 57 44.4	40 35 46	0.0570	0.25L	1.07	2.29	0.11	8.76	8.45	11.82	11.48
NGC 6890	20 14 50.0	−44 57 20	0.0080	0.46	0.76	3.66	8.59	7.14	6.43	10.12	10.21
IRAS 2025−818	20 25 23.9	−81 52 40	0.0344	0.32	0.67	1.16	1.21L	7.68	7.78	11.11	10.87
ESO 234−G50	20 32 13.4	−50 22 14	0.0087	0.25L	0.26	0.68	1.00	7.06	7.18	9.57	9.47
UGC 11630	20 45 00.0	00 13 35	0.0122	0.35L	0.42	1.14	1.13L	6.64	6.42	10.09	9.93
IC 5063	20 48 11.9	−57 15 27	0.0113	1.07	3.91	5.34	4.17	8.13	7.85	10.85	10.51
IRAS 2143−045	21 43 06.2	−04 32 18	0.1034	0.25L	0.57	0.96	1.13L	8.78	8.60	12.05	11.81
IC 5135	21 45 19.6	−35 11 07	0.0160	0.63	2.16	16.41	25.52	7.28	7.78	11.33	11.39
NGC 7172	21 59 07.6	−32 06 42	0.0086	0.44	0.76	5.71	12.29	...	...	10.32	10.45
IRAS 2201+033	22 01 47.2	03 19 15	0.0611	0.66L	0.74	1.13	1.24	8.96	8.57	11.66	11.38
NGC 7212	22 04 33.9	09 59 20	0.0260	0.34L	0.74	2.95	4.96	8.15	8.39	11.10	11.09
IRAS 2205−519W	22 05 19.1	−51 58 38	0.0648	0.11	0.39	0.62	0.62	8.55	8.47	11.44	11.16
Frl 357	22 23 39.0	−70 39 00	0.0280	0.25L	0.25L	0.76	1.55	...	...	10.62	10.60
NGC 7314	22 33 00.0	−26 18 30	0.0060	0.27L	0.66	3.33	14.41	6.40	6.72	9.82	10.06
NGC 7319	22 33 50.0	33 43 29	0.0220	0.25L	0.29L	0.64	2.89	7.63	7.39	10.40	10.50
Mrk 917	22 38 48.2	31 54 30	0.0250	0.32L	0.69	3.86	5.58	7.89	7.96	11.13	11.15
Mrk 308	22 39 31.2	20 00 04	0.0233	0.25L	0.78	2.49	2.66	8.11	8.20	10.96	10.85
IRAS 2302+120	23 02 26.5	12 03 09	0.0074	0.75	3.33	11.93	24.26	5.15	5.33	10.61	10.63
NGC 7496	23 06 59.0	−43 42 00	0.0500	0.33	1.53	8.42	14.81	8.14	9.21	12.09	12.14
NGC 7592	23 15 47.3	−04 41 22	0.0223	0.36	1.10	7.95	10.36	6.36	6.41	11.31	11.35
NGC 7590	23 16 11.0	−42 30 40	0.0050	0.52	0.85	7.27	17.43	6.35	6.88	9.94	10.10
NGC 7674	23 25 24.4	08 30 13	0.0290	0.67	1.89	5.58	8.14	8.66	8.25	11.52	11.44
NGC 7682	23 26 31.0	03 15 30	0.0170	0.51	1.16	7.29	9.53	7.86	7.45	11.05	11.07
MCG +02-60-017	23 44 36.6	15 19 06	0.0260	0.25L	1.23	4.14	3.39	6.40	6.85	11.27	11.14
IRAS 2353+299	23 53 10.9	29 55 54	0.0307	0.45L	0.39	0.70	1.00L	8.57	8.32	10.78	10.59

Note.—Units of right ascension are hours, minutes, and seconds, and units of declination are degrees, arcminutes, and arcseconds. Luminosities are calculated for $H_0 = 50$ km s^{-1} Mpc^{-1}; "L" stands for upper limit detection, a colon (:) stands for uncertain value, and an asterisk (*) following the redshift value indicates the objects for which the distance has been calculated via the distance modulus (Sandage & Tammann 1981).

tion. In this paper, only the observed (not corrected for internal reddening) [O III]$_{\lambda 5007}$ and Hα luminosities are used,[2] as well as the far-infrared luminosities calculated for the "warm" and "cold" spectral ranges, L_{IR}^{W} and L_{IR}^{C}, respectively (see § 3.1 for their definitions). These luminosities (relative to the solar value) are calculated for $H_0 = 50$ km s^{-1} Mpc^{-1} and are given in Table 1.

Sample B contains a compilation of 336 galaxies selected from the available literature on AGNs, resulting in a total of 136 Seyfert 1 galaxies and 200 Seyfert 2 galaxies. Data for

[2] For objects with multicomponent emission lines, the quoted luminosity corresponds to the sum of all components.

Seyfert 1 galaxies are listed in Table 2, and those for Seyfert 2 galaxies are in Table 3.

Information on emission-line luminosities for most of the galaxies in sample B have been found in the available literature (e.g., Kriss, Canizares, & Ricker 1980; Rudy 1984; Osterbrock & de Robertis 1985; Véron-Cetty & Véron 1986; Dahari & De Robertis 1988; Morris & Ward 1988; Lipari, Bonatto, & Pastoriza 1991; de Grijp et al. 1992; and Mulchaey et al. 1996) and in the NASA/IPAC Extragalactic Database (NED).[3]

3. INFRARED PROPERTIES

3.1. *Far-Infrared Luminosities*

In order to characterize the temperature regimes of both types of Seyfert galaxies, the far-infrared luminosity with respect to two different spectral ranges are calculated: a "cold" one ($L_{\rm IR}^{C}$) based on the *IRAS* bands at 60 and 100 μm and a "warm" one ($L_{\rm IR}^{W}$) based on the 25 and 60 μm bands (the 12 μm *IRAS* band is not used because most of these observations are upper limits or uncertain). These luminosities are calculated as follows: $\log (L_{\rm IR}^{W}) = 47.16 + 2 \log [z(1+z)] + \log (2.4S_{25} + S_{60})$ ergs s^{-1} and $\log (L_{\rm IR}^{C}) = 46.73 + 2 \log [z(1+z)] + \log (2.58S_{60} + S_{100})$ ergs s^{-1}, where S_{25}, S_{60}, and S_{100} are the flux densities in janskys at 25, 60, and 100 μm, respectively.

Combining all the galaxies of our two samples, we are left with 140 Seyfert 1 galaxies and 234 Seyfert 2 galaxies. Both groups have objects spanning a rather large interval in far-infrared luminosity, e.g., for the Seyfert 1 galaxies, $7.6 \leq \log (L_{\rm IR}^{W}/L_{\odot}) \leq 12.6$ and for the Seyfert 2 galaxies, $8.7 \leq \log (L_{\rm IR}^{W}/L_{\odot}) \leq 12.4$. For the combined sample, we have produced the histograms shown in Figure 1 for the number of objects with $L_{\rm IR}^{W}$ and $L_{\rm IR}^{C}$ within a given luminosity bin. Gaussians have been fitted to each histogram in order to better characterize the distributions. Although a selection effect certainly occurred, in the sense that only the brightest galaxies in the infrared have been observed by the *IRAS* satellite, we conclude from the analysis of the histograms in Figure 1 that the type 1 and 2 Seyfert galaxies of our samples are nearly undistinguishable on the basis of their far-infrared luminosities alone. Despite the large-scale similarity among the distributions, some small differences can be noted: in the warm range, the peak of the Seyfert 1 distribution ($8.13 \times 10^{10}\ L_{\odot}$) is $\approx$5% brighter than that of the Seyfert 2 galaxies ($7.76 \times 10^{10}\ L_{\odot}$), while in the cold range, the peak of the Seyfert 2 distribution ($6.46 \times 10^{10}\ L_{\odot}$) is $\approx$10% brighter than that of the Seyfert 1 galaxies ($5.89 \times 10^{10}\ L_{\odot}$).

Luminosities in each individual *IRAS* band can be used to search for systematic differences between type 1 and 2 Seyfert galaxies. For this analysis, flux densities marked as uncertain or as upper limits (Tables 1, 2, and 3) have been excluded, and the resulting luminosity distributions are shown in the form of histograms in Figure 2. Seyfert types are clearly differentiated in the 12 μm luminosity histograms, in the sense that the peak of the Seyfert 1 distribution is shifted toward higher luminosities with respect to Seyfert 2 galaxies. A similar, although much smaller, trend can be seen in the 25 μm luminosity histograms. In the 60 μm luminosity histograms, it is the peak of the Seyfert 2 galaxies that is slightly shifted toward higher luminosities with respect to the Seyfert 1 galaxies, and in the 100 μm luminosity histograms, no clear difference can be noted between type 1 and 2 Seyfert galaxies.

We conclude from the above analysis that if these far-infrared luminosities are mainly the result of radiation reemitted by dust, these histograms indicate that dust at higher temperatures would be more important for Seyfert 1 galaxies than for Seyfert 2 galaxies.

3.2. *Host Galaxy's Contribution to the Far-Infrared Emission*

Besides the hot emission from dust directly heated by the AGN, there exists a contribution from a cold component peaking near 100 μm coming from the host galaxy, which is important mainly for AGNs with $z > 0.014$ for which the large *IRAS* diaphragms must have covered off-nuclear regions.

In normal spiral galaxies, the observed 60 and 100 μm fluxes can be almost entirely accounted for by a combination of relatively cool (20–25 K) dust heated by the interstellar radiation field and warmer dust heated by O and B stars (Walterbos & Greenwalt 1996). The cool dust contribution can amount to $\approx$50% of the flux at these two bands but decreases for shorter wavelengths. Because of the presence of other, more important heating mechanisms in Seyfert galaxies, the cool dust contribution to the infrared flux must be smaller in these objects than in normal spirals, especially at 12 μm. Indeed, a study with small apertures in a limited sample of Seyferts by Roche et al. (1984) shows that, on average, $\approx$80% of the 12 μm *IRAS* flux in Seyfert 1 galaxies comes from the nucleus, as compared with $\approx$60% in Seyfert 2 galaxies.

To estimate the effect of this cool dust component on Seyfert-pure color indices, we have used the empirical spectra (Rowan-Robinson & Crawford 1989) of typical Seyfert and normal disk components. Considering the observed flux at some frequency ν as the sum of the Seyfert and disk components, $S_{\nu} = S_{\nu}^{S} + S_{\nu}^{D}$, any color index (for $\lambda_2 > \lambda_1$) can be written as follows:

$$
\begin{aligned}
-\alpha(\lambda_2, \lambda_1) &= \log \left(\frac{S_{\nu 2}}{S_{\nu 1}}\right) \Big/ \log \left(\frac{\lambda_2}{\lambda_1}\right) \\
&= \log \left(\frac{S_{\nu 2}^{S} + S_{\nu 2}^{D}}{S_{\nu 1}^{S} + S_{\nu 1}^{D}}\right) \Big/ \log \left(\frac{\lambda_2}{\lambda_1}\right) \\
&= \log \left(\frac{S_{\nu 2}^{S}}{S_{\nu 1}^{S}}\right) \Big/ \log \left(\frac{\lambda_2}{\lambda_1}\right) \\
&= -\alpha^{S}(\lambda_2, \lambda_1) + K^{D}(\lambda_2, \lambda_1) , \qquad (1)
\end{aligned}
$$

where $\alpha^{S}(\lambda_2, \lambda_1)$ is the Seyfert color index and $K^{D}(\lambda_2, \lambda_1)$ is the correction due to the cold disk component. As an example, if the cold component contributes to the observed flux at 12 μm with $\approx$10% relative to the Seyfert component, and taking into account the flux ratios tabulated in Rowan-Robinson & Crawford (1989), the above corrections to the color indices at the *IRAS* bands are

$$
\begin{aligned}
\alpha(100, 60) &= \alpha^{S}(100, 60) - 1.53 , \\
\alpha(60, 25) &= \alpha^{S}(60, 25) - 0.42 , \\
\alpha(25, 12) &= \alpha^{S}(25, 12) + 0.08 . \qquad (2)
\end{aligned}
$$

[3] The NASA/IPAC Extragalactic Database (NED) is operated by the Jet Propulsion Laboratory, California Institute of Technology, under contract with the National Aeronautics and Space Administration.

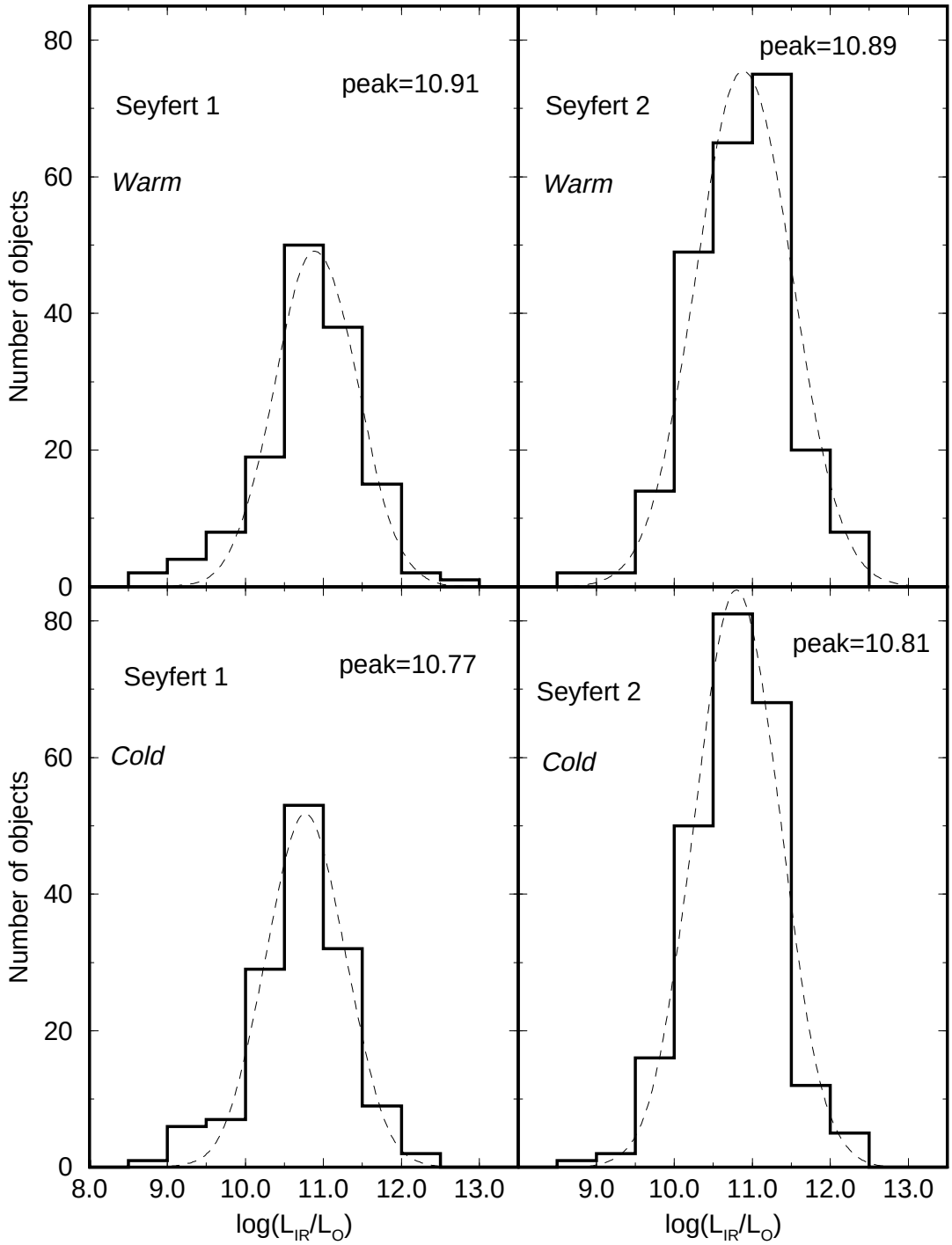

FIG. 1.—Histograms for the number of objects with a given L_{IR}^{C} and L_{IR}^{W}. *Left-hand panels*: Seyfert 1 galaxies; *right-hand panels*: Seyfert 2 galaxies. The cold far-infrared luminosity is shown in the bottom panels, and the warm one is shown in the top panels. The short-dashed lines show the best Gaussian fit to each distribution, with peaks at, for Seyfert 1 galaxies, $L_{IR}^{C} = 5.89 \times 10^{10}\ L_{\odot}$ and $L_{IR}^{W} = 8.13 \times 10^{10}\ L_{\odot}$ and, for Seyfert 2 galaxies, $L_{IR}^{C} = 6.46 \times 10^{10}\ L_{\odot}$ and $L_{IR}^{W} = 7.76 \times 10^{10}\ L_{\odot}$.

Thus, the cold disk component turns the color indices $\alpha(100, 60)$ and $\alpha(60, 25)$ more negative (redder) than the Seyfert-pure ones.

3.3. *Galaxy Groups*

The color index $\alpha(100, 60)$ is that which presents the largest range of values for the galaxies of our samples. So instead of considering the 374 galaxies individually, we have divided the whole interval of $\alpha(100, 60)$ values in bins of 0.5 dex and then calculated the average value of $\alpha(25, 12)$ and $\alpha(60, 25)$ for the objects in each bin. It is important to stress that only flux densities not marked as uncertain or upper limit detections have been considered in this process. As a result, seven groups have been derived for both types of Seyferts.

Table 4 gives information on the resulting groups: the columns give the group designation; the number of galaxies in each group; the average values of the color indices $\alpha(25, 12)$, $\alpha(60, 25)$, and $\alpha(100, 60)$, along with their standard deviations; the average *IRAS* flux densities at 12, 25, and 100

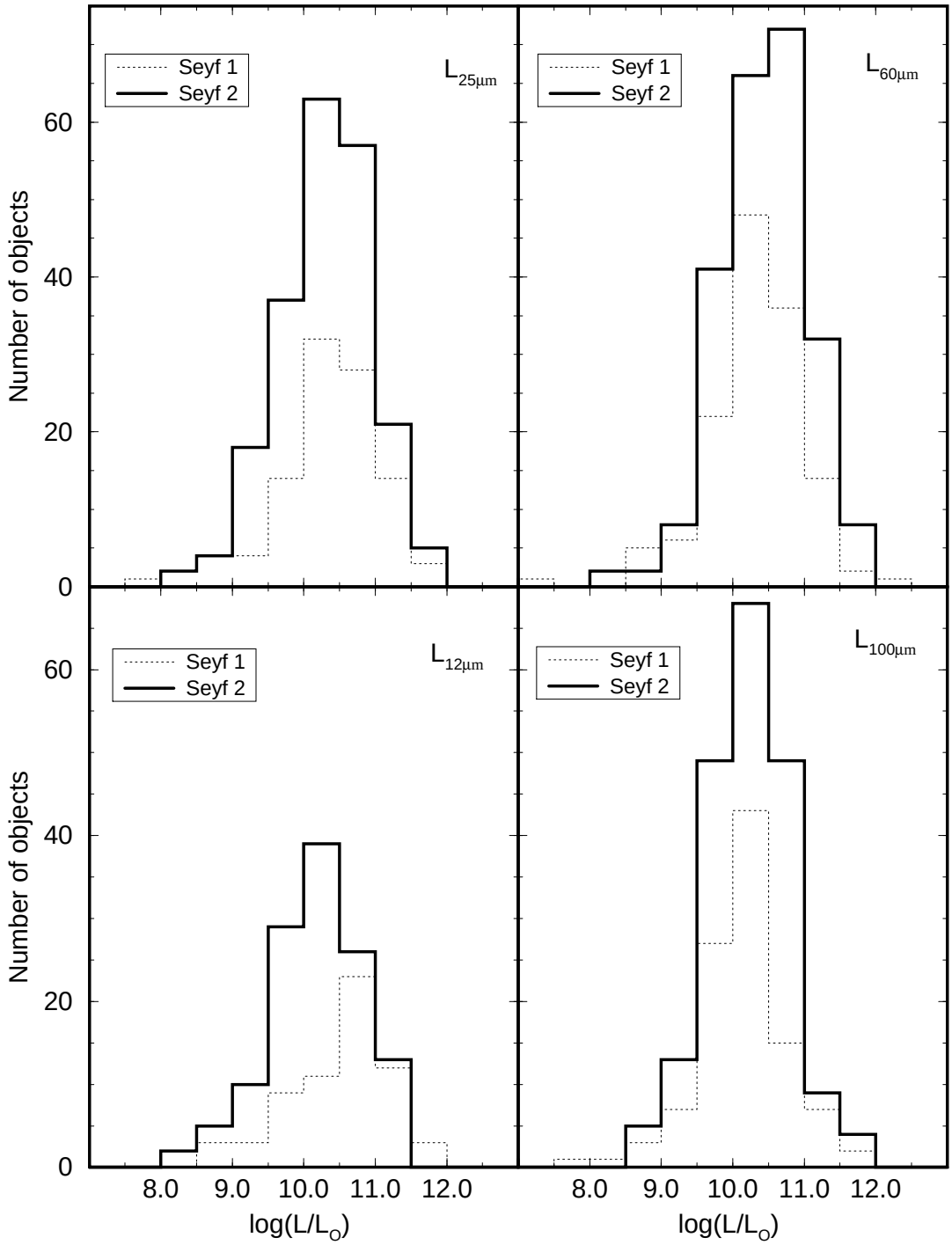

FIG. 2.—Histograms for the number of objects with a given luminosity bin in each individual *IRAS* band. Seyfert 1 galaxies are shown as a dashed line, and the Seyfert 2 galaxies are shown as a solid line. Seyfert types clearly differ in the 12 μm histogram, where Seyfert 1 distribution is biased toward higher luminosities than that of Seyfert 2 galaxies.

μm (normalized to $S_{60} = 1$ Jy); and the average values of $\log (L_{\rm IR}^{W}/L_{\odot})$ and $\log (L_{\rm IR}^{C}/L_{\odot})$. The quoted uncertainties reflect the internal error for the average value for each group. Notice that the groups follow an approximately increasing sequence in $L_{\rm IR}^{W}$ and $L_{\rm IR}^{C}$. The similarities between type 1 and 2 Seyferts can again be appreciated by the average values of the derived group flux densities, which are plotted in Figure 3. In this figure we see that from group 1 (G1) to group 7 (G7), the main characteristic of both types of Seyferts is the decreasing ratio S_{100}/S_{60}; notice also that G1 is very steep for the Seyfert 2 galaxies. Dust at lower temperatures must be more important to G1 in Seyfert 2 galaxies ($S_{100}/S_{60} \approx 4.3$) than in Seyfert 1 galaxies ($S_{100}/S_{60} \approx 3.8$). From G1 to G6, the cool dust contribution decreases and the hot dust dominates.

4. DISCUSSION

4.1. *Dust Emission Model*

The dust emission and spatial distribution model follows,

TABLE 4

AVERAGE VALUES DERIVED FOR THE SEYFERT GROUPS

Group	N	$\langle\alpha(25, 12)\rangle$	$\langle\alpha(60, 25)\rangle$	$\langle\alpha(100, 60)\rangle$	$\langle S_{12}\rangle$	$\langle S_{25}\rangle$	$\langle S_{100}\rangle$	$\left\langle \log\left(\frac{L_{IR}^{W}}{L_{\odot}}\right)\right\rangle$	$\left\langle \log\left(\frac{L_{IR}^{C}}{L_{\odot}}\right)\right\rangle$
				Seyfert 1 Galaxies					
1	2	...	$-2.26 \pm$ ...	-2.63 ± 0.05	...	$0.14 \pm$ ...	3.83 ± 0.10	$9.12 \pm$ ...	9.77 ± 0.56
2	13	-0.45 ± 0.25	-2.44 ± 0.55	-2.31 ± 0.14	0.12 ± 0.12	0.28 ± 0.15	3.26 ± 0.23	9.78 ± 0.15	10.27 ± 0.33
3	22	-0.73 ± 0.63	-1.10 ± 0.71	-1.72 ± 0.13	0.30 ± 0.13	0.37 ± 0.25	2.42 ± 0.16	10.56 ± 0.48	10.55 ± 0.42
4	18	-0.88 ± 0.41	-1.05 ± 0.55	-1.23 ± 0.14	0.25 ± 0.14	0.45 ± 0.20	1.88 ± 0.14	10.81 ± 0.45	10.68 ± 0.57
5	19	-1.20 ± 0.42	-0.84 ± 0.58	-0.78 ± 0.11	0.24 ± 0.14	0.53 ± 0.22	1.49 ± 0.08	11.00 ± 0.62	10.91 ± 0.58
6	16	-1.24 ± 0.53	-1.12 ± 0.59	-0.27 ± 0.17	0.22 ± 0.13	0.42 ± 0.18	1.15 ± 0.10	11.20 ± 0.56	11.05 ± 0.54
7	8	-1.26 ± 0.52	-0.95 ± 0.57	0.21 ± 0.14	0.34 ± 0.17	0.49 ± 0.24	0.90 ± 0.07	11.19 ± 0.62	10.98 ± 0.70
				Seyfert 2 Galaxies					
1	4	$-0.76 \pm$ ...	-1.71 ± 1.32	-2.85 ± 0.15	$0.04 \pm$ ...	0.34 ± 0.36	4.29 ± 0.31	10.27 ± 0.94	10.46 ± 0.62
2	10	-0.72 ± 0.47	-2.05 ± 1.01	-2.21 ± 0.13	0.06 ± 0.02	0.28 ± 0.16	3.10 ± 0.20	10.12 ± 0.42	10.14 ± 0.55
3	27	-0.72 ± 0.45	-1.93 ± 0.59	-1.69 ± 0.09	0.13 ± 0.10	0.23 ± 0.13	2.36 ± 0.12	10.42 ± 0.47	10.47 ± 0.42
4	35	-1.18 ± 0.59	-1.67 ± 0.57	-1.21 ± 0.13	0.11 ± 0.08	0.27 ± 0.15	1.86 ± 0.13	10.80 ± 0.51	10.80 ± 0.51
5	55	-1.45 ± 0.34	-1.28 ± 0.34	-0.74 ± 0.14	0.14 ± 0.10	0.37 ± 0.17	1.46 ± 0.10	10.93 ± 0.51	10.84 ± 0.51
6	42	-1.72 ± 0.75	-1.26 ± 0.58	-0.24 ± 0.14	0.18 ± 0.19	0.37 ± 0.18	1.13 ± 0.08	11.17 ± 0.53	11.03 ± 0.57
7	17	-1.71 ± 0.16	-1.01 ± 0.50	0.35 ± 0.46	0.16 ± 0.07	0.45 ± 0.18	0.95 ± 0.28	11.16 ± 0.51	10.94 ± 0.53

NOTE.—*IRAS* flux densities are normalized to $S_{60} = 1$ Jy; N is the number of galaxies in each group with good-quality data.

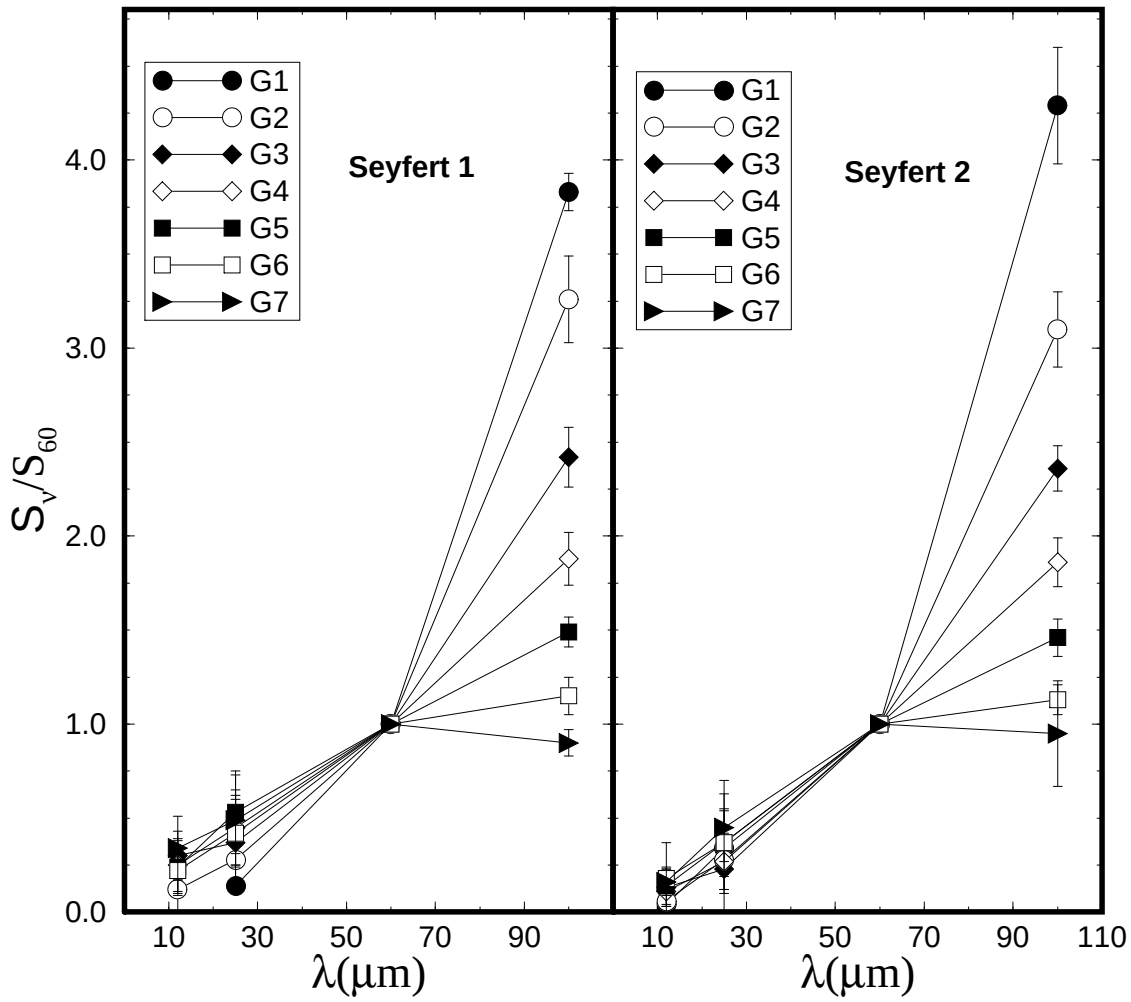

FIG. 3.—Average far-infrared spectra of the derived Seyfert groups. Flux densities at the *IRAS* bands (relative to the flux at $\lambda = 60$ μm) are plotted against wavelength. *Left-hand panel*: Seyfert 1 galaxies; *right-hand panel*: Seyfert 2 galaxies.

in general, the outlines presented by Barvainis (1987), Rees et al. (1969), Panagia (1975), and Bollea & Cavaliere (1976).

In this model the dust can be found uniformly distributed around the central source or concentrated in spherically symmetric distributed clouds. Another plausible alternative is for the dust to be distributed with a special geometry, such as a disk or torus in which the optical depth to UV/optical photons is very large. The radial profile of the grain number density follows a power law with slope β, $\eta(r) \propto r^{-\beta}$, and the grains are exposed solely to the CIS's UV/optical continuum, so that grains at different distances from the nucleus will come to thermal equilibrium at different temperatures, thus producing a radial temperature profile (for further details on the model, see Barvainis 1987). We reproduce here only the following results: (*a*) the total energy absorbed by dust and reemitted in the infrared ($L_{\rm IR}$) is related to the total incident UV luminosity ($L_{\rm UV}$) as

$$\frac{L_{\rm IR}}{L_{\rm UV}} = \frac{\Omega}{4\pi}\,(1 - e^{-\tau_{\rm ef}})\,, \qquad (3)$$

where Ω is the solid angle subtended by the dust distribution at the nucleus and $\tau_{\rm ef}$ is the effective optical depth to the incident UV/optical continuum along our line of sight, and (*b*) the inner radius (r_1, in parsecs) of the dust distribution is defined as the distance from the CIS at which the grains would come to thermal equilibrium at its characteristic evaporation temperature ($T_{\rm ev}$), and for dust with a grain radius $a = 0.05$ μm, r_1 is given by

$$r_1 \approx 1.3 L_{\rm UV46}^{1/2}\, T_{1500}^{-2.8}\ {\rm pc}\,, \qquad (4)$$

where $L_{\rm UV46}$ is the CIS's total UV luminosity in units of 10^{46} ergs s^{-1} and T_{1500} is the evaporation temperature in units of 1500 K.[4]

4.2. *Average Far-Infrared Colors of the Groups*

For the interpretation of the average colors of the groups, we make use of diagrams for the *IRAS* bands that take into account hot dust emission models (§ 4.1) and the effects of cool dust (§ 3.2). The diagram that best reproduces the whole range of colors for the groups is the one for α(100, 60) × α(25, 12) and dust models for grains with evaporation temperature $T_{\rm ev} = 1500$ K and dust distribution characterized by $r_2/r_1 = 10^4$. This diagram for the observed colors is shown in Figure 4, in which Seyfert 1 groups are united by a solid line and Seyfert 2 groups are united by a dotted line. For comparison, the colors of a blackbody at different temperatures have been plotted as a long-dashed line, while the solid diagonal line corresponds to the colors of a pure power law, $F_\nu \propto \nu^\alpha$. The ratio r_2/r_1, where r_2 is the outer radius of the dust distribution, is related to the extension of the distribution (see eq. [4]). Colors of dust-pure models calculated according to Barvainis (1987) are shown as diamonds linked by a dotted line and are identified by the corresponding grain number density slope, β. For completeness we include dust models for uniform grain density ($\beta = 0.0$) and high grain concentration ($\beta = 2.0$).

Each Seyfert group in Figure 4 is identified by its number (according to Table 4), and the corresponding standard deviations are plotted as vertical lines (Seyfert 1 galaxies, *solid line*; Seyfert 2 galaxies, *dotted line*) over the average value. Clearly, both curves are very similar, although Seyfert 2 groups tend to have larger scatter. In terms of α(100, 60), there is no significant difference in the colors of groups with the same number between type 1 and 2 Seyferts, but with respect to α(25, 12), Seyfert 2 groups are redder than the corresponding ones of Seyfert 1 groups. Type 1 and 2 Seyfert groups are distributed in Figure 4 in sequences of decreasing far-infrared luminosity with increasing distance to the colors of dust-pure models.

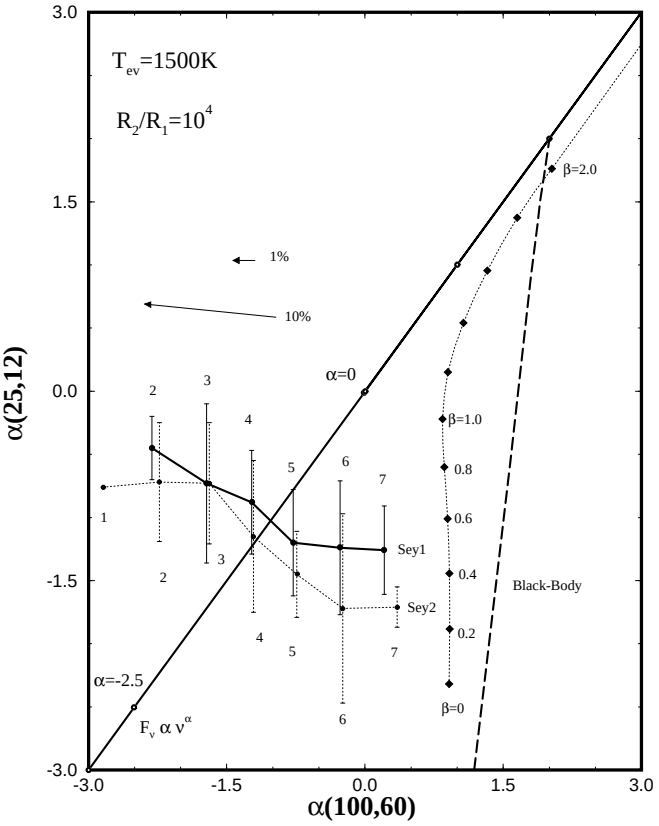

FIG. 4.—Seyfert groups are plotted on this color-color diagram for dust models with $T_{\rm ev} = 1500$ K and $r_2/r_1 = 10^4$. Type 1 Seyferts are united by a solid line, and type 2 galaxies are joined by a dotted line. Vertical lines indicate the standard deviations in each group. Arrows indicate the effect on Seyfert-pure colors produced by cool dust contributions at 12 μm of 1% and 10%.

Group colors plotted in this diagram (Fig. 4) correspond to the observed ones, which, according to the discussion presented in § 3.2, are the result of the Seyfert-pure (in the present work, AGN-heated dust) colors added to those produced by the contribution of cool dust. In this case, the arrows in Figure 4 illustrate the changes that cool dust contributions of 1% and 10% at 12 μm would produce on Seyfert-pure colors. The effect of a 1% contribution is negligible, only the Seyfert-pure α(100, 60) would be shifted (reddened) 0.31 units to the left, and a 10% contribution would shift the Seyfert-pure α(100, 60) by 1.53 units to the left. The ratio $r_2/r_1 = 10^4$, together with equation (4) (for a typical UV luminosity, $L_{\rm UV46} \approx 0.1$), implies a dust distribution reaching a distance of $\approx 10^3$ pc around the nucleus.

Following the simple hypothesis that the observed colors of Seyfert galaxies are the result of dust directly heated by the AGN combined with some fraction of emission from

[4] The most common dust grains, graphite, have $T_{\rm ev} \approx 1500$ K (Mathis, Rumpl, & Nordsiek 1977; Draine & Lee 1984).

cool dust, the whole range of observed colors shown in Figure 4 can be well reproduced by dust models with slope β between 0.2 and 0.6 and cool dust contributions (at 12 μm) of at most $\approx$20%. In fact, for both type 1 and 2 Seyferts, a very small cool dust contribution would be enough to explain the colors of the most luminous groups (group 7), whereas a fraction of about 20% would be necessary for the least luminous ones (groups 1 and 2). The cool dust contribution becomes less important to the observed colors as the Seyfert luminosity (AGN-heated dust) increases.

4.3. *Optical and Far-Infrared Luminosities: Interpretation*

For the galaxies with available optical data, we have produced the histograms shown in Figure 5 for the number of objects with a given ratio of the far-infrared luminosities with respect to $L_{\rm H\alpha}$ (*left-hand panels*) and $L_{\rm [O\ III]}$ (*right-hand panels*). Let us first examine the ratios $L_{\rm IR}^{W}/L_{\rm H\alpha}$ and $L_{\rm IR}^{C}/L_{\rm H\alpha}$. Gaussian fits to the distributions yield peaks $L_{\rm IR}^{C}/L_{\rm H\alpha} = 1.12 \times 10^{2}$ and $1.29 \times 10^{3}\ L_{\odot}$ and $L_{\rm IR}^{W}/L_{\rm H\alpha} = 1.38 \times 10^{2}$ and $1.45 \times 10^{3}\ L_{\odot}$, respectively, for type 1 and 2 Seyferts.

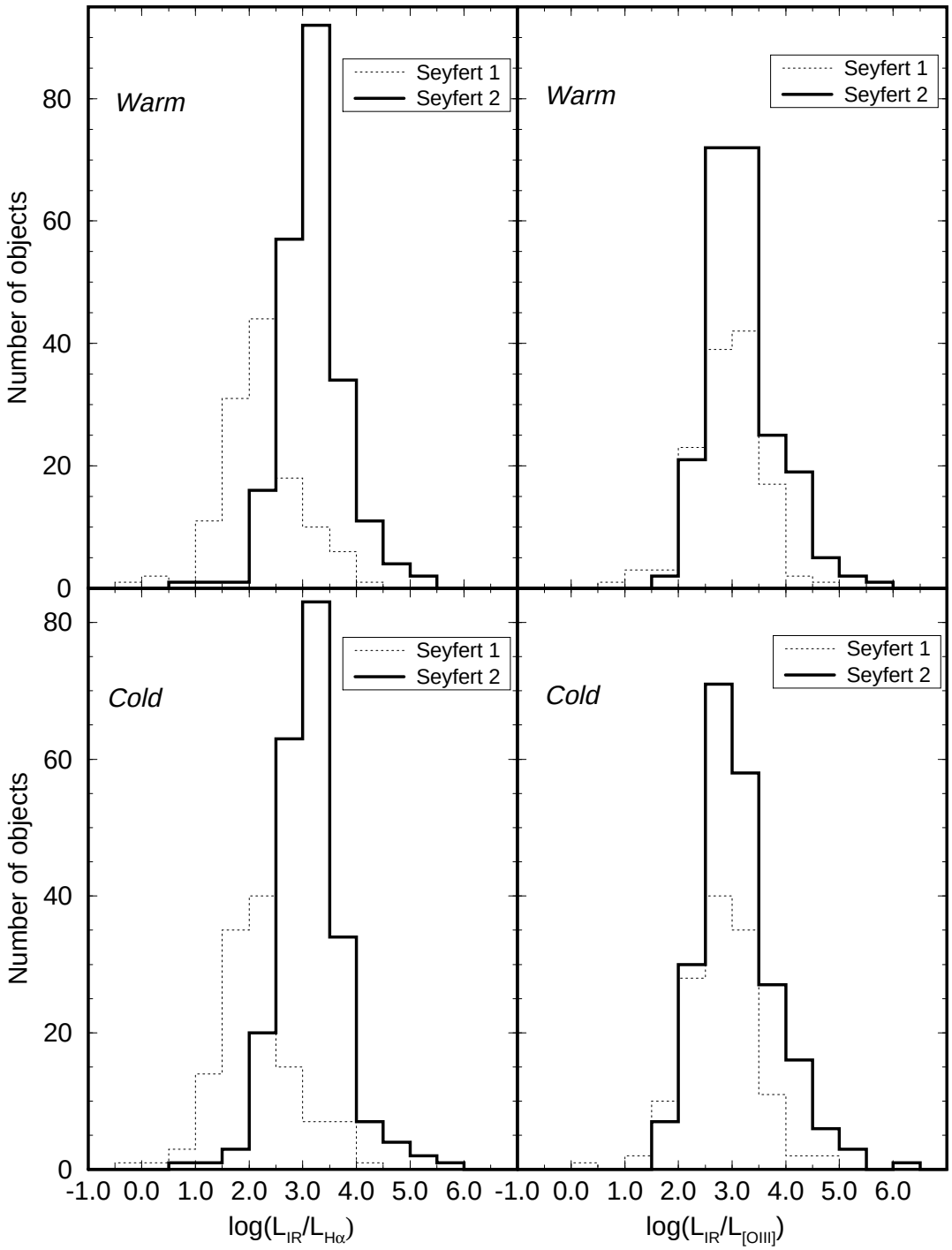

FIG. 5.—Histograms for the number of objects with a given ratio of far-infrared luminosity with respect to $L_{\rm H\alpha}$ (*left-hand panels*) and $L_{\rm [O\ III]}$ (*right-hand panels*). Luminosity ratios with respect to the warm and cold far-infrared ranges are shown, respectively, in the top and bottom panels. Seyfert 1 distributions are shown as a dotted line, and Seyfert 2 distributions appear as a straight line.

These histograms can be interpreted according to the following picture. Let us assume a galaxy having a CIS in its nucleus emitting a continuum of UV/optical photons; the CIS is surrounded by a region of a hot and dense gas (typically $N_e > 10^9$ cm^{-3} and $T_e > 10^4$ K) with dimension $r \leq 1$ pc in which are emitted the broad lines, mainly H I lines (the broad-line region, or BLR); the BLR can be surrounded by a spherical distribution (uniform or concentrated in clouds) of dust with a low τ_{UV} (or, alternatively, a disk or torus with $\tau_{UV} \gg 1$ whose plane forms some angle with our line of sight); farther from the nucleus, at $r \sim 1 - 10^3$ pc, is the narrow line region (NLR) containing gas and dust.

In the most general situation, the CIS emits photons isotropically that first ionize the BLR gas, and then the fraction of these photons not absorbed by the gas together with BLR photons arrive to the dust. The dust will absorb a fraction of the incident photons $\propto(1 - e^{-\tau_{UV}})$ (spherical case) or $\propto(\Omega/4\pi)$ (disk/torus) that are reemitted in the infrared and eventually escape the galaxy. For a low τ_{UV} (or $\Omega/4\pi \ll 1$) a large number of photons will get to the NLR, ionize the gas therein, and produce the narrow lines. In this case we would expect a proportionality between the ionizing photon flux and the resulting Hα luminosity: $L_{H\alpha} \propto L_{UV}$. Thus, an approximately constant ratio $L_{IR}/L_{H\alpha}$ (i.e., a strong peak in the distribution) would imply that L_{IR}/L_{UV} is nearly constant. This last result, taken together with equation (3) and associated with the presence of a well-defined peak in the $L_{IR}/L_{H\alpha}$ distribution for the Seyfert 1 galaxies, indicates that τ_{UV} or $\Omega/4\pi$ takes only on a typical range of values.

Particularly noticeable in the Seyfert 1 galaxies is an extension of the distributions toward the region of large values of the ratios, which can be accounted for by objects having the BLR substantially more obscured by dust, a likely situation in transition Seyferts, which do not have or only show evidence of a broad component in Hα. Alternatively, there could be a direct contribution to the far-infrared from the UV/optical power law in these objects. A similar, although less important, asymmetry is observed in the Seyfert 2 distributions, which could reflect the presence of other mechanisms that produce infrared radiation, such as circumnuclear star formation.

With the assumption that the dust has a larger τ_{UV} (or the disk/torus obscures the BLR more efficiently), BLR photons emitted in our direction will be almost completely absorbed and reemitted in the infrared. In this case, only narrow lines will be observed, thus resulting in a deficiency of optical line photons relative to the previous situation. This seems to be the case with Seyfert 2 galaxies, in which broad lines are not observed. In fact, the peaks of the Seyfert 2 distributions lie at a ratio $\approx$10 times larger than that of the Seyfert 1 galaxies.

With respect to [O III]$_{\lambda 5007}$, the histograms for type 1 and 2 Seyferts are very similar, even considering the two far-infrared luminosity ranges. Mulchaey et al. (1996) found a similar result for a smaller number of objects and argued that this is consistent with the hypothesis that the O III$_{\lambda 5007}$ and far-infrared emissions are isotropic in both types of Seyferts. Similar to Mulchaey et al. (1996) we find that the $L_{IR}^W/L_{[O\ III]}$ and $L_{IR}^C/L_{[O\ III]}$ distributions for the Seyfert 2 galaxies are slightly broader than those for the Seyfert 1 galaxies, and this difference could be explained by the presence of an additional warm component in the Seyfert 2 galaxies (e.g., circumnuclear star formation) or, alternatively, by partial obscuration of the [O III]–emitting regions by a torus. However, in our case we caution that the difference in width could be due to the larger number of type 2 Seyfert galaxies with respect to type 1 Seyferts in our samples.

[O III] lines are emitted mostly outside the BLR.[5] If the dust is very efficient in obscuring the BLR, fewer photons will be left to ionize the gas outside the BLR and produce narrow lines such as [O III] and Hα. In this case the distributions of $L_{IR}^W/L_{[O\ III]}$ and $L_{IR}^C/L_{[O\ III]}$ should be similar to those with respect to $L_{H\alpha}$, and this is exactly the situation observed in the Seyfert 2 galaxies (Fig. 5). The same does not apply to the Seyfert 1 galaxies: since they have the BLR unobstructed or only partially obscured, the contribution from broad Hα components produces low values of the ratios $L_{IR}^W/L_{H\alpha}$ and $L_{IR}^C/L_{H\alpha}$ (Fig. 5).

These facts allow us to say that type 1 and 2 Seyferts are the same kind of objects, with the latter ones having the Seyfert nucleus and BLR "hidden" by a dust distribution. Antonucci (1984) and Antonucci & Miller (1985) have shown that the nuclear regions of the broad-line radio galaxy 3C 234 and the Seyfert 2 NGC 1068 are probably obscured by optical and geometrically thick disks. NGC 1068 presents broad emission lines in polarized light and would look like a Seyfert 1 when viewed from unobstructed directions. Besides, Krolik & Begelman (1986) postulated the presence of a wind in NGC 1068 due to the heating of molecular clouds by the nuclear continuum, implying an extended region containing hot dust.

If a Seyfert nucleus and a BLR are hidden by a thick accretion torus, for example, then biconical radiation fields could be produced by collimation due to the torus walls. This kind of structure was observed in the central regions ($r \leq 2$ kpc) of the nearby Seyfert 2 galaxies NGC 1365 and NGC 7582 through narrow-band images of O III$_{\lambda 5007}$ in emission (Storchi-Bergmann & Bonatto 1991). In both galaxies a ratio $L_{IR}/L_H \approx 10$ was found, where L_H is the luminosity of the observed UV/optical continuum, thus showing that part of the radiation heating the dust is not being observed. Besides, Véron et al. (1980) found evidence of a broad component of Hα in NGC 1365 that could indicate the presence of a hidden Seyfert nucleus. Further examples of this kind of situation can be found in Wilson, Ward, & Hanniff (1988), Wilson & Tsvetanov (1994), and Wilson (1996).

5. CONCLUSION

In this work we study moderately large samples of type 1 and 2 Seyfert galaxies through optical and far-infrared *IRAS* data. The far-infrared properties of these objects have been characterized through the *IRAS* luminosities L_{IR}^W (25–60 μm) and L_{IR}^C (60–100 μm) and color indices derived for the *IRAS* bands. Below we summarize our main results.

1. We have built histograms for the number of objects with a given L_{IR}^C and L_{IR}^W and found that type 1 and 2 Seyferts present nearly the same distributions. Small differences in the maximum of the distributions indicate the presence of dust at higher temperatures in type 1 than in type 2 Seyferts.

[5] However, photoionization models of Kwan & Krolik (1979, 1981) indicate the formation of [O III] lines in high N_e clouds close to the BLR; the literature is substantial in examples of broad [O III]$_{\lambda 5007}$ in Seyfert 1 galaxies (Bonatto & Pastoriza 1990).

2. Differences found in luminosity distributions for the individual *IRAS* bands also point to the same conclusion.

3. The galaxies have been separated according to the observed far-infrared color index $\alpha(100, 60)$, which results in seven different groups for type 1 and 2 Seyferts. Similar to the far-infrared luminosity distributions, we show that the groups for type 1 and 2 Seyferts cannot be distinguished on the basis of their observed color indices.

4. With a simple model in which the observed colors of Seyferts result from dust directly heated by the AGN (the Seyfert-pure component) combined with cool dust emission (originating in the host galaxy), the whole range of colors exhibited by our groups can be explained by dust models with β values from 0.2 to 0.6 and cool dust contributions (to the 12 μm flux) from a few to a maximum of about 20%.

5. From histograms for the number of objects with a given ratio of $L_{\rm IR}^{W}$ and $L_{\rm IR}^{C}$ to $L_{\rm H\alpha}$ and $L_{\rm [O\ III]}$, we show that the same model of a nuclear source and BLR surrounded by a dust distribution can be applied to type 1 and 2 Seyferts, varying only some model conditions to explain the latter type, such as the use of a larger optical depth or a more efficient obscuration.

6. At least from the point of view of the far-infrared Hα and [O III]$_{\lambda 5007}$ emissions, we find no evidence of systematic differences among the type 2 Seyferts of our sample, thus arguing against the existence of "true" Seyfert 2 galaxies, i.e., objects that do not have a BLR.

We thank the Brazilian institution CNPq for partial support of the observing runs at Cerro Tololo Inter-American Observatory (CTIO), and C. B. thanks the Fundação de Amparo à Pesquisa do Estado do Rio Grande do Sul (FAPERGS) for 3 months of financial support. We are indebted to Dr. S. Lipari for making available the Complejo Astronomico El Leoncito data and acknowledge the support of the CTIO staff during the observations and initial data reductions. Thanks to the referee, Dr. R. Barvainis, for helpful suggestions that improved the paper.

REFERENCES

Antonucci, R. R. J. 1984, ApJ, 278, 499
Antonucci, R. R. J., & Miller, J. S. 1985, ApJ, 297, 621
Barvainis, R. 1987, ApJ, 320, 537
———. 1990, ApJ, 353, 419
Bollea, D., & Cavaliere, A. 1976, A&A, 49, 313
Bonatto, C. J., & Pastoriza, M. G. 1990, ApJ, 353, 445
Dahari, O., & De Robertis, M. M. 1988, ApJSS, 67, 249
de Grijp, M. H. K., Keel, W. C., Miley, G. K., Goudfrooij, P., & Lub, J. 1992, A&AS, 96, 389
de Grijp, M. H. K., Miley, G. K., & Lub, J. 1987, A&AS, 70, 95
Draine, B. T., & Lee, H. M. 1984, ApJ, 285, 89
Joint *IRAS* Science Working Group, *IRAS* Point Source Catalogue 1985 (Washington: US Government Printing Office)
Jones, B., Worrall, D. M., Rodriguez-Espinosa, J. M., Stein, W. A., & Gillet, F. C. 1984, PASP, 96, 692
Kriss, G. A., Canizares, C. R., & Ricker, G. R. 1980, ApJ, 242, 492
Krolik, J. H., & Begelman, M. C. 1986, ApJ, 308, L55
Kwan, J., & Krolik, J. H. 1979, ApJ, 233, L91
———. 1981, ApJ, 250, 478
Lipari, S., Bonatto, C. J., & Pastoriza, M. G. 1991, MNRAS, 253, 19
MacAlpine, G. M. 1985, in Astrophysics of Active Galaxies and Quasi-stellar Objects, ed. Joseph S. Miller (Mill Valley: Univ. Science), 259
Mathis, J. S., Rumpl, W., & Nordsiek, K. H. 1977, ApJ, 217, 425
Morris, S. L., & Ward, M. J. 1988, MNRAS, 230, 639
Mulchaey, J. S., Koratkar, A., Ward, M. J., Wilson, A. S., Whittle, M., Antonucci, R. R. J., Kinney, A. L., & Hurt, T. 1996, ApJ, 436, 586
Neugebauer, G., Becklin, E. E., Oke, J. B., & Searle, L. 1976, ApJ, 205, 29
Osterbrock, D., & de Robertis, M. M. 1985, PASP, 97, 1129
Pacholczyck, A. G., & Wisniewski, W. Z. 1967, ApJ, 147, 394
Panagia, N. 1975, A&A, 42, 139
Rees, M. J., Silk, J. I., Werner, M. W., & Wickramasinghe, N. C. 1969, Nature, 223, 788
Rieke, G. H. 1978, ApJ, 226, 550
Roche, P. F., Aitken, D. K., Phillips, M. M., & Whitmore, B. 1984, MNRAS, 207, 35
Rowan-Robinson, M., & Crawford, J. 1989, MNRAS, 238, 523
Rudy, R. J. 1984, ApJ, 284, 33
Sandage, A., & Tammann, G. A. 1981, The Revised Shapley-Ames Catalog of Bright Galaxies (Washington: Carnegie Inst. Washington), 635
Storchi-Bergmann, T., & Bonatto, C. J. 1991, MNRAS, 250, 138
Tonry, J., & Davis, M. 1979, AJ, 84, 1511
Véron, P., Lindblad, P. O., Zuiderwijk, E. J., Véron, M. P., & Adam, G. 1980, A&A, 87, 245
Véron-Cetty, M.-P., & Véron, P. 1986, A&AS, 66, 335
Walterbos, R. A. M., & Greenwalt, B. 1996, ApJ, 460, 696
Wampler, E. J. 1968, ApJ, 154, L53
———. 1971, ApJ, 164, 1
Ward, M., Elvis, M., Fabbiano, G., Carleton, N. P., Willner, S. P., & Lawrence, A. 1987, ApJ, 315, 74
Wilson, A. S. 1996, Vistas Astron., 40, 63
Wilson, A. S., & Tsvetanov, Z. I. 1994, AJ, 107, 1227
Wilson, A. S., Ward, M. J., & Hanniff, C. A. 1988, ApJ, 334, 121